

A NONLINEAR FLUID-STRUCTURE INTERACTION PROBLEM IN COMPLIANT ARTERIES TREATED WITH VASCULAR STENTS

MARTINA BUKAČ, SUNČICA ČANIĆ, AND BORIS MUHA

ABSTRACT. We study a nonlinear fluid-structure interaction problem between an incompressible, viscous fluid in 3D and an elastic structure whose Lamé elastic parameters, thickness and density are all functions of space allowing jump discontinuities. This problem is motivated by studying the interaction between blood flow and arterial walls treated with vascular prostheses called stents. A stent is a metallic mesh-like tube used to prop the clogged arteries open. The Navier-Stokes equations for an incompressible, viscous fluid are used to model blood flow, and the cylindrical Koiter shell equations with discontinuous coefficients are used to model the elastic properties of arterial walls treated with stents. The fluid and structure are coupled via two coupling conditions evaluated at the moving fluid-structure interface. No assumption on axial symmetry is used in the model. We prove the existence of a weak solution to the underlying nonlinear 3D moving-boundary problem, and design a loosely-coupled partitioned scheme (β -scheme) for its solution. The numerical scheme was motivated by the main steps in the constructive existence proof. The existence proof shows that the proposed numerical β -scheme converges to a weak solution of the nonlinear problem. This is the first convergence result for the proposed partitioned β -scheme. Several numerical examples are presented where different stent configurations are considered. The numerical fluid-structure interaction solutions clearly show that the presence of a stent induces wave reflections in arterial walls, and significant flow disturbances, especially near the proximal site of the stent.

1. INTRODUCTION

This work is motivated by fluid-structure interaction problems arising in cardiovascular repair called coronary angioplasty with stenting. Coronary angioplasty is a minimally invasive procedure which is used to treat coronary artery disease (CAD). Coronary artery disease (clogging, or stenosis of coronary artery) is the major cause of heart attacks, the leading cause of death in the US. Coronary angioplasty entails inserting a catheter with a mounted balloon which is inflated to widen the lumen of a diseased artery (the area occupied by blood) and restore normal blood flow. To prop the arteries open a metallic mesh tube called a stent is inserted at the location of the narrowing. See Figure 1. To understand

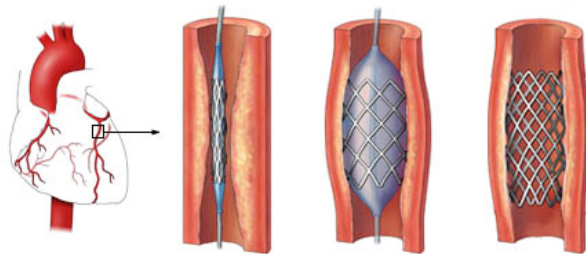


FIGURE 1. Coronary angioplasty with stenting.

which stent is most appropriate for a particular lesion and a particular coronary artery geometry, cardiovascular specialists are interested in the analysis of global mechanical properties of coronary stents currently available on the US market. The overall mechanical properties of stents depend on the material used in the stent production (e.g., stainless steel, cobalt-chromium alloy, nitinol, etc), and on

2000 *Mathematics Subject Classification.* 35R37; 35M33.

Key words and phrases. Fluid-structure interaction; Nonlinear moving-boundary problem; Existence of a solution; Cardiovascular stents; Kinematically coupled β -scheme.

the way how the local stent components, called stent struts, are distributed within a stent to form the global stent net structure.

Of particular interest is the study of the performance of different stents inserted in a human artery and their response to the stresses exerted by the blood flow and by the arterial tissue. This defines a fluid-structure interaction problem between an incompressible, viscous fluid such as blood, and an elastic structure, such as arterial wall treated with a vascular stent. The presence of a stent in the arterial wall can be modeled by modifying the elastic Lamé constants in the structural model, and by changing the thickness and the density of the elastic material where the stent is located. In this work the structure, which corresponds to the arterial wall with a stent in it, will be modeled by a linearly elastic Koiter shell model with the Lamé coefficients, the structure density, and the structure thickness all being functions of space, and exhibiting jump discontinuities at the points where the stent edges are located. See Figure 2. The blood flow will be modeled using the Navier-Stokes equations for an incompressible, viscous fluid in 3D. No axial symmetry will be assumed in the existence proof. The fluid and structure are fully coupled

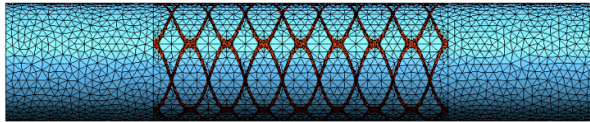


FIGURE 2. An example of a stented artery domain with a computational mesh.

via two coupling conditions: the kinematic coupling condition describing continuity of velocity at the fluid-structure interface (i.e., the no-slip condition), and the dynamic coupling condition describing the second Newton’s law of motion stating that the elastodynamics of the thin fluid-structure interface is driven by the jump in the normal stress across the interface. For simplicity, we will be assuming that the external normal stress is equal to zero. The fluid flow is driven by the difference in the dynamic pressure between the inlet and outlet of the fluid domain.

We study the existence of a weak solution and a construction of a numerical scheme for this nonlinear fluid-structure interaction problem by designing a constructive existence proof which is based on the time discretization via operator splitting. The main steps in the proof define a partitioned, loosely coupled scheme for the numerical simulation of this nonlinear FSI problem. Therefore, we present in this manuscript the existence analysis, a loosely-coupled partitioned numerical scheme, and numerical simulations for the nonlinear FSI problem describing the interaction between blood flow and arterial wall treated with a vascular stent. The existence proof shows that the corresponding numerical scheme converges, as the time-discretization step tends to zero, to a weak solution of the underlying FSI problem.

The time-discretization via operator splitting separates the fluid and structure sub-problems, which are split in such a way that the energy of the semi-discretized problem mimics the energy of the coupled *continuous* problem. This way the difficulties associated with the *added mass effect* [19] are being avoided, and only one iteration between the fluid and structure sub-problems is needed to get a stable, convergent scheme. We have used similar strategies in the past to study various FSI problems [58, 62, 59, 60]. The novelties of the present work are:

- (1) The coefficients in the structure model are functions of space and are bounded in L^∞ .
- (2) The operator splitting strategy in the existence proof is different from the previously used strategies in [62, 59, 60] in that the fluid and structure sub-problems do not communicate only via the initial data, but also via the jump in the normal fluid stress across the fluid-structure interface, which is now being distributed between the fluid and structure sub-problems with the “weight” $\beta \in [0, 1)$. Therefore, this is a *modification* of the so called Lie splitting, which was used in our previous works [62, 59, 60]. This modification provides higher accuracy in the numerical calculation of solutions [15].
- (3) The numerical simulations with different stent configurations and material properties provide new information about the influence of stent geometry and material properties on the overall, global performance of stents interacting with blood flow.

2. LITERATURE REVIEW

Fluid-structure interaction problems have been extensively studied by many authors. The development of numerical solvers for FSI problems has become particularly active since the 1980s, while the development of well-posedness theory started about 20 years ago. Despite significant progress, many questions related to well-posedness theory for FSI problems still remain a challenge. The field has evolved from first studying FSI between an incompressible, viscous fluid and rigid immersed structures, to considering compliant (elastic/viscoelastic) structures. The coupling between the fluid and compliant structure was first assumed to take place along a fixed fluid domain boundary (linear coupling), and later extended to the coupling evaluated at a deformed fluid-structure interface, giving rise to an additional nonlinearity in the problem (nonlinear coupling).

FSI problems coupling the Navier-Stokes equations with linear elasticity where the coupling was calculated at a fixed fluid domain boundary were considered in [33], in [20] where a simplified FSI model was considered and a stent example was presented, and in [8, 9, 51] where an additional nonlinear coupling term was added at the interface. Well-posedness for a completely linearized FSI problem was considered in [11]. A study of well-posedness for FSI problems between an incompressible, viscous fluid and an elastic/viscoelastic structure with nonlinear coupling evaluated at a moving interface started with the result by daVeiga [10], where existence of a strong solution was obtained locally in time for an interaction between a $2D$ fluid and a $1D$ viscoelastic string, assuming periodic boundary conditions. This result was extended by Lequeurre in [54, 55], where the existence of a unique, local in time, strong solution for any data, and the existence of a global strong solution for small data, was proved in the case when the structure was modeled as a clamped viscoelastic beam. The existence of a global in time solution to the fluid-viscoelastic beam system was proved in [41]. D. Coutand and S. Shkoller proved existence, locally in time, of a unique, regular solution for an interaction between a viscous, incompressible fluid in $3D$ and a $3D$ structure, immersed in the fluid, where the structure was modeled by the equations of linear [28], or quasi-linear [29] elasticity. In the case when the structure (solid) is modeled by a linear wave equation, I. Kukavica et al. proved the existence, locally in time, of a strong solution, assuming lower regularity for the initial data [49, 47, 45]. A similar result for compressible flows can be found in [50]. In [66] Raymond et al. considered a FSI problem between a linear elastic solid immersed in an incompressible viscous fluid, and proved the existence and uniqueness of a strong solution. A fluid-structure interaction between a viscous, incompressible fluid in $3D$, and $2D$ elastic shells was considered in [23, 22] where existence, locally in time, of a unique regular solution was proved. All the above mentioned existence results for strong solutions are local in time. Recently, in [46] a global existence result for small data was obtained for a similar moving boundary FSI problem assuming some additional interface and structure damping terms. We also mention that the works of Shkoller et al., and Kukavica et al. were obtained in the context of Lagrangian coordinates, which were used for both the structure and fluid problems.

In the context of weak solutions, the following results have been obtained. Continuous dependence of weak solutions on initial data for a fluid structure interaction problem with a free boundary type coupling condition was studied in [43]. Existence of a weak solution for a FSI problem between a $3D$ incompressible, viscous fluid and a $2D$ viscoelastic plate was considered by Chambolle et al. in [21], while Grandmont improved this result in [40] to hold for a $2D$ elastic plate. These results were extended to a more general geometry in [53], and then to the case of generalized Newtonian fluids in [52], and to a non-Newtonian shear dependent fluid in [56]. In these works existence of a weak solution was proved for as long as the elastic boundary does not touch "the bottom" (rigid) portion of the fluid domain boundary.

Muha and Čanić recently proved the existence of weak solutions to a class of FSI problems modeling the flow of an incompressible, viscous, Newtonian fluid flowing through a $2D$ cylinder whose lateral wall was modeled by either the linearly viscoelastic, or by the linearly elastic Koiter shell equations [62], assuming nonlinear coupling at the deformed fluid-structure interface. The fluid flow boundary conditions were not periodic, but rather, the flow was driven by a time-dependent dynamic pressure data. The methodology of proof in [62] was based on a semi-discrete, operator splitting Lie scheme, which was used in [42] to design a stable, loosely coupled partitioned numerical scheme, called the kinematically coupled scheme (see also [13]). Ideas based on the Lie operator splitting scheme were also

used by Temam in [69] to prove the existence of a solution to the nonlinear Carleman equation. These results were recently extended by Muha and Čanić to a FSI problem with two structural layers [59], 3D non-radially symmetric case [58], a semi-linear cylindrical Koiter shell [61], and the case where the structure and the fluid are coupled via the Navier slip boundary condition [60].

The numerical method development for FSI problems involving incompressible, viscous fluids and elastic structures has featured monolithic and partitioned approaches. Monolithic schemes are based on solving the entire coupled system together, while in partitioned scheme the system is decoupled in some way and reduced to solving two or more sub-problems. While there is extensive literature on both approaches, we focus our attention on partitioned schemes since they are directly related to the scheme presented in the present paper. For a more extensive literature review we refer the reader to [14, 17].

In classical partitioned schemes such as, e.g., the Dirichlet-Neumann scheme, the coupled FSI problem is partitioned into a fluid and a structure sub-problem with the structure velocity used as Dirichlet data for the fluid sub-problem, while the structure is loaded by the fluid stress, previously calculated in the fluid sub-problem. Unfortunately, when fluid and structure have comparable densities, which is the case in the blood flow application, this simple strategy of separating the fluid from structure suffers from severe stability issues associated with the added mass effect [19]. To get around these difficulties, and to retain the main advantages of loosely-coupled partitioned schemes such as modularity, simple implementation, and low computational costs, several new partitioned algorithms have been proposed recently [4, 13, 12, 42, 64, 35, 36, 3, 5, 63, 31, 30, 6, 7]. Among those scheme is the so called Kinematically Coupled β -Scheme, introduced by Bukač, Čanić et al. in [13, 12], and applied to FSI problems with thin elastic and viscoelastic structures, modeled by the membrane or shell equations. It was shown in [70] that the scheme does not suffer from the instabilities caused by the added mass effect even for the parameters associated with the blood flow applications. Stability is achieved by combining the structure inertia with the fluid sub-problem as a Robin boundary condition, to mimic the energy balance of the continuous, coupled problem, while the structure problem is treated separately. The Robin-type boundary condition in the fluid sub-problem only depends on the structure thickness and density, in contrast with the coupled momentum method by Figueroa [37], where the whole structure equation is included in the fluid problem, leading to an ill-conditioned system more comparable to the one obtained by a monolithic formulation. Numerically, it was shown in [13] that the accuracy of the Kinematically-Coupled β -scheme with $\beta = 1$ was comparable to that of the monolithic scheme by Badia, Quaini, and Quarteroni in [5] when applied to a nonlinear benchmark FSI problem in hemodynamics, introduced by Formaggia et al. in [38]. Recently, first order convergence of the scheme was proved rigorously in [15]. A different approach to increasing the accuracy of the classical kinematically-coupled scheme was recently proposed by Fernández [35]. Their modified kinematically-coupled scheme, called “the incremental displacement-correction scheme” treats the structure displacement explicitly in the fluid sub-step and then corrects it in the structure sub-step. They showed that the accuracy of the incremental displacement-correction scheme is first-order in time.

These recent results indicate that the kinematically-coupled scheme and its modifications provide an appealing way to study multi-physics problems involving FSI. Indeed, due to its simple implementation, modularity, and very good performance, modifications of this scheme have been used by several authors to study different multi-physics problems involving FSI, such as FSI with poroelastic structures [16], and FSI involving non-Newtonian fluids [44, 56].

In the present manuscript we design a modification of the originally proposed β -scheme, and use it to study FSI problems involving vascular devices called stents. We prove, for the first time, that the β -scheme converges to a weak solution of the underlying nonlinear FSI problem with a stent.

3. MODEL DESCRIPTION

We study a fluid-structure interaction problem between an incompressible, viscous Newtonian fluid modeled by the Navier-Stokes equations in 3D, and an elastic structure, modeled by the cylindrical Koiter shell equations, with parameters that are not constant, but are functions of space. No axial symmetry is assumed in the problem.

To simplify calculations, we will be using Cartesian coordinates $(z, x, y) \in \mathbb{R}^3$ to describe the fluid equations, and cylindrical coordinates $(z, r, \theta) \in \mathbb{R}^3$ to describe the structure. A function f given in

Cartesian coordinates defines a function

$$\tilde{f}(z, r, \theta) = f(z, x, y)$$

defined in cylindrical coordinates. Since no confusion is possible we will omit the superscript $\tilde{}$ and both functions, f and \tilde{f} , will be denoted by f .

The structure is modeled as a clamped cylindrical Koiter shell of length L and reference radius of the middle surface equal to R . The reference configuration of the shell is a straight cylinder:

$$(3.1) \quad \Gamma = \{\mathbf{x} = (R \cos \theta, R \sin \theta, z) \in \mathbb{R}^3 : (z, \theta) \in \omega := (0, L) \times (0, 2\pi)\}.$$

We will be assuming that the shell thickness h is a strictly positive bounded function on $\omega = (0, L) \times (0, 2\pi)$, i.e. $h \in L^\infty(\omega)$, $h \geq \alpha > 0$ a.e. in Γ . In the numerical examples, presented below in Section 8, thickness h of the structure will be larger at the points where the stent struts are located.

The displacement from the reference configuration Γ will be denoted by $\boldsymbol{\eta} = \boldsymbol{\eta}(t, z, \theta) = (\eta_z, \eta_\theta, \eta_r)$. We will be assuming that only the radial component of displacement is different from zero, and will be denoting that component by $\eta(t, z, \theta) := \eta_r(t, z, \theta)$, so that $\boldsymbol{\eta} = \eta \mathbf{e}_r$, where $\mathbf{e}_r = \mathbf{e}_r(\theta) = (\cos \theta, \sin \theta, 0)^t$ is the unit vector in the radial direction. Notice that the displaced cylindrical Koiter shell does not have to be axially symmetric.

A Koiter shell can undergo stretching of the middle surface, measured by the change of metric tensor, and flexure or bending (shell effects), measured by the change of curvature tensor. By assuming only the radial component of displacement $\eta = \eta(t, r, \theta)$ to be different from zero, the linearized change of metric tensor $\boldsymbol{\gamma}$, and the linearized change of curvature tensor $\boldsymbol{\rho}$, are given by the following:

$$(3.2) \quad \boldsymbol{\gamma}(\eta) = \begin{pmatrix} 0 & 0 \\ 0 & R\eta \end{pmatrix}, \quad \boldsymbol{\rho}(\eta) = \begin{pmatrix} -\partial_z^2 \eta & -\partial_{z\theta}^2 \eta \\ -\partial_{z\theta}^2 \eta & -\partial_\theta^2 \eta + \eta \end{pmatrix}.$$

The corresponding elastic energy of the deformed shell is then given by [26, 24, 25, 48]:

$$(3.3) \quad E_{el}(\eta) = \int_\omega \frac{h}{4} \mathcal{A} \boldsymbol{\gamma}(\eta) : \boldsymbol{\gamma}(\eta) R dz d\theta + \int_\omega \frac{h^3}{48} \mathcal{A} \boldsymbol{\rho}(\eta) : \boldsymbol{\rho}(\eta) R dz d\theta,$$

where h is the (variable) thickness of the shell, and \mathcal{A} is the elasticity tensor defining the elastic properties of the shell via:

$$(3.4) \quad \mathcal{A} \mathbf{E} = \frac{4\lambda\mu}{\lambda + 2\mu} (\mathbf{A}^c \cdot \mathbf{E}) \mathbf{A}^c + 4\mu \mathbf{A}^c \mathbf{E} \mathbf{A}^c, \quad \mathbf{E} \in \text{Sym}(\mathcal{M}_2), \quad \text{with } \mathbf{A}^c = \begin{pmatrix} 1 & 0 \\ 0 & \frac{1}{R^2} \end{pmatrix},$$

where \mathbf{A}^c is the contravariant metric tensor of the undeformed cylinder. The coefficients $\mu = \mu(z, \theta)$ and $\lambda = \lambda(z, \theta)$ are the Lamé coefficients, which depend on $(z, \theta) \in \omega$, and are such that $\lambda, \mu \in L^\infty(\omega)$, $\lambda, \mu \geq \alpha > 0$ a.e. on ω . The Lamé coefficients will be significantly higher in the region where the stent struts are located, describing higher stiffness due to the presence of the stent struts. The following notation in (3.4) is used for the scalar product:

$$(3.5) \quad \mathbf{A} : \mathbf{B} := \text{Tr}(\mathbf{A} \mathbf{B}^T) \quad \mathbf{A}, \mathbf{B} \in \mathbf{M}_2(\mathbb{R}) \cong \mathbb{R}^4.$$

Given a force $\mathbf{f} = f \mathbf{e}_r$, with surface density f (the radial component), the loaded shell deforms under the applied force. In our problem f will correspond to the jump in the normal stress across the shell, i.e., the difference in the fluid normal stress and the external normal stress. From the elastic energy (3.3), the corresponding displacement η satisfies the following elastodynamics problem for the cylindrical linearly elastic Koiter shell, written in weak form: Find $\eta \in H_0^2(\omega)$ such that

$$(3.6) \quad \int_\omega \rho_K h \partial_t^2 \eta \psi R + \int_\omega \frac{h}{2} \mathcal{A} \boldsymbol{\gamma}(\eta) : \boldsymbol{\gamma}(\psi) R + \int_\omega \frac{h^3}{24} \mathcal{A} \boldsymbol{\rho}(\eta) : \boldsymbol{\rho}(\psi) R = \int_\omega f \psi R, \quad \forall \psi \in H_0^2(\omega),$$

where the Koiter shell density ρ_K is also a function of $(z, \theta) \in \omega$, and is such that $\rho_K(z, \theta) \in L^\infty(\omega)$, $\rho_K \geq \alpha > 0$. Again, the Koiter shell density will be higher in the region where the stent struts are located. To simplify notation we introduce the elastic operator \mathcal{L} :

$$(3.7) \quad \int_\omega \mathcal{L} \eta \psi := \int_\omega \frac{h}{2} \mathcal{A} \boldsymbol{\gamma}(\eta) : \boldsymbol{\gamma}(\psi) R + \int_\omega \frac{h^3}{24} \mathcal{A} \boldsymbol{\rho}(\eta) : \boldsymbol{\rho}(\psi) R, \quad \forall \psi \in H_0^2(\omega),$$

so that the above weak formulation can be written as

$$(3.8) \quad \int_{\omega} \rho_K h \partial_t^2 \eta \psi R \, dz d\theta + \int_{\omega} \mathcal{L} \eta \psi \, dz d\theta = \int_{\omega} f \psi R \, dz d\theta, \quad \forall \psi \in H_0^2(\omega).$$

In our simulations, the Lamé coefficients will be piecewise constant functions, having a jump discontinuity at the edges where the stent struts are located. An explicit form for the operator \mathcal{L} used in the numerical simulations will be given in Section 8. Thus, the elastodynamics problems for a clamped cylindrical Koiter shell with non-constant coefficients reads:

$$(3.9) \quad \begin{cases} \rho_K h \partial_t^2 \eta + \mathcal{L} \eta = f & \text{on } \omega, \\ \eta = \frac{\partial \eta}{\partial \mathbf{n}} = 0 & \text{on } \partial \omega, \\ \eta = \eta_0 & \text{for } t = 0, \end{cases}$$

where \mathcal{L} is given by the weak form (3.7).

The fluid problem is defined on a domain which depends on time and is not known *a priori*:

$$\Omega_{\eta}(t) = \{(z, x, y) \in \mathbb{R}^3 : \sqrt{x^2 + y^2} < R + \eta(t, z, \theta), z \in (0, L)\},$$

with the lateral boundary given by:

$$\Gamma_{\eta}(t) = \{(z, x, y) \in \mathbb{R}^3 : \sqrt{x^2 + y^2} = R + \eta(t, z, \theta), z \in (0, L)\}.$$

The inlet and outlet sections of the fluid domain boundary will be denoted by $\Gamma_{in} = \{0\} \times (0, R)$, $\Gamma_{out} = \{L\} \times (0, R)$. See Figure 3. We are interested in studying a dynamic pressure-driven flow

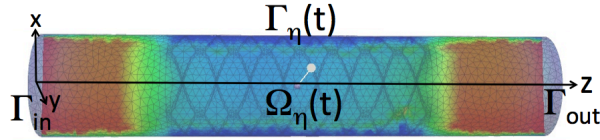


FIGURE 3. Fluid domain and notation.

through $\Omega_{\eta}(t)$ of an incompressible, viscous fluid modeled by the Navier-Stokes equations which are given in Cartesian coordinates:

$$(3.10) \quad \left. \begin{aligned} \rho_f (\partial_t \mathbf{u} + \mathbf{u} \cdot \nabla \mathbf{u}) &= \nabla \cdot \sigma, \\ \nabla \cdot \mathbf{u} &= 0, \end{aligned} \right\} \text{ in } \Omega_{\eta}(t), \quad t \in (0, T),$$

where ρ_f denotes the fluid density, \mathbf{u} fluid velocity, p fluid pressure, $\sigma = -p\mathbf{I} + 2\mu_F \mathbf{D}(\mathbf{u})$ is the fluid Cauchy stress tensor, μ_F is the kinematic viscosity coefficient, and $\mathbf{D}(\mathbf{u}) = \frac{1}{2}(\nabla \mathbf{u} + \nabla^t \mathbf{u})$ is the symmetrized gradient of \mathbf{u} . At the inlet and outlet boundaries we prescribe zero tangential velocity and dynamic pressure $p + \frac{\rho_f}{2}|u|^2$ (see e.g. [27]):

$$(3.11) \quad \left. \begin{aligned} p + \frac{\rho_f}{2}|u|^2 &= P_{in/out}(t), \\ \mathbf{u} \times \mathbf{e}_z &= 0, \end{aligned} \right\} \text{ on } \Gamma_{in/out},$$

where $P_{in/out} \in L_{loc}^2(0, \infty)$ are given. Therefore the fluid flow is driven by a prescribed dynamic pressure drop, and the flow enters and leaves the fluid domain orthogonally to the inlet and outlet boundary.

The coupling between the fluid and structure is defined by two sets of boundary conditions satisfied at the lateral boundary $\Gamma_{\eta}(t)$. They are the kinematic and dynamic lateral boundary conditions describing continuity of velocity (the no-slip condition), and the Second Newton's Law of motion stating that the elastodynamics of the structure is driven by the jump in the normal stress acting on the structure. By assuming that the external stress to the structure is zero, in Lagrangian coordinates, with $(z, \theta) \in \omega$, and $t \in (0, T)$, the conditions read:

- **The kinematic condition:**

$$(3.12) \quad \partial_t \eta(t, z, \theta) \mathbf{e}_r(\theta) = \mathbf{u}(t, z, R + \eta(t, z, \theta), \theta),$$

where $\mathbf{e}_r(\theta) = (\cos \theta, \sin \theta, 0)^t$ is the unit vector in the radial direction.

• **The dynamic condition:**

$$(3.13) \quad \rho_K h \partial_t^2 \eta + \mathcal{L} \eta = -J(t, z, \theta) (\sigma \mathbf{n})|_{(t, z, R + \eta(t, z, \theta))} \cdot \mathbf{e}_r(\theta),$$

where \mathcal{L} is defined by (3.7), and

$$J(t, z, \theta) = \sqrt{(1 + \partial_z \eta(t, z, \theta))^2 (R + \eta(t, z, \theta))^2 + \partial_\theta \eta(t, z, \theta)^2}$$

denotes the Jacobian of the composition of the transformation from Eulerian to Lagrangian coordinates and the transformation from cylindrical to Cartesian coordinates.

System (3.10)–(3.13) is supplemented with the following **initial conditions**:

$$(3.14) \quad \mathbf{u}(0, \cdot) = \mathbf{u}_0, \quad \eta(0, \cdot) = \eta_0, \quad \partial_t \eta(0, \cdot) = v_0.$$

Additionally, we will be assuming that the initial data satisfies the following compatibility conditions:

$$(3.15) \quad \begin{aligned} \mathbf{u}_0(z, R + \eta_0(z), \theta) \cdot \mathbf{n}(z, \theta) &= v_0(z, \theta) \mathbf{e}_r(\theta) \cdot \mathbf{n}(z, \theta), \quad z \in (0, L), \theta \in (0, 2\pi), \\ \eta_0 &= 0, \quad \text{on } \partial\omega, \\ R + \eta_0(z, \theta) &> 0, \quad z \in [0, L], \theta \in (0, 2\pi). \end{aligned}$$

In summary, we study the following nonlinear fluid-structure interaction problem with discontinuous structure coefficients: *Find* $\mathbf{u} = (u_z(t, z, x, y), u_x(t, z, x, y), u_y(t, z, x, y)), p(t, z, x, y)$, and $\eta(t, z, \theta)$ such that

$$(3.16) \quad \left. \begin{aligned} \rho_f (\partial_t \mathbf{u} + (\mathbf{u} \cdot \nabla) \mathbf{u}) &= \nabla \cdot \boldsymbol{\sigma} \\ \nabla \cdot \mathbf{u} &= 0 \end{aligned} \right\} \text{ in } \Omega_\eta(t), \quad t \in (0, T),$$

$$(3.17) \quad \left. \begin{aligned} \mathbf{u} &= \partial_t \eta \mathbf{e}_r, \\ \rho_K h \partial_t^2 \eta + \mathcal{L} \eta &= -J \boldsymbol{\sigma} \mathbf{n} \cdot \mathbf{e}_r, \end{aligned} \right\} \text{ on } (0, T) \times \omega,$$

$$(3.18) \quad \left. \begin{aligned} p + \frac{\rho_f}{2} |u|^2 &= P_{in/out}(t), \\ \mathbf{u} \times \mathbf{e}_z &= 0, \end{aligned} \right\} \text{ on } (0, T) \times \Gamma_{in/out},$$

$$(3.19) \quad \left. \begin{aligned} \mathbf{u}(0, \cdot) &= \mathbf{u}_0, \\ \eta(0, \cdot) &= \eta_0, \\ \partial_t \eta(0, \cdot) &= v_0. \end{aligned} \right\} \text{ at } t = 0,$$

where \mathcal{L} is given by (3.7), with the coefficients that are L^∞ -functions of $(z, \theta) \in \omega$, and $\rho_K, h \in L^\infty(\omega)$.

3.1. Energy inequality. Assuming sufficient regularity, we formally derive an energy inequality for the coupled FSI problem (3.16)–(3.19). To simplify notation, we introduce the following energy norms defined by the membrane and flexural effects of the linearly elastic Koiter shell with L^∞ coefficients:

$$(3.20) \quad \|f\|_\gamma := \int_\omega \frac{h}{4} \mathcal{A} \boldsymbol{\gamma}(f) : \boldsymbol{\gamma}(f) R dz d\theta, \quad \|f\|_\sigma := \int_\omega \frac{h^3}{48} \mathcal{A} \boldsymbol{\sigma}(f) : \boldsymbol{\sigma}(f) R dz d\theta.$$

Notice that norm $\|\cdot\|_\gamma$ is equivalent to the standard $L^2(\omega)$ norm, and that norm $\|\cdot\|_\sigma$ is equivalent to the standard $H_0^2(\omega)$ norm.

Proposition 3.1. *Assuming sufficient regularity, solutions of (3.16)–(3.19) satisfy the following energy estimate:*

$$(3.21) \quad \frac{d}{dt} (E_{kin}(t) + E_{el}(t)) + D(t) \leq C(P_{in}(t), P_{out}(t)),$$

where

$$(3.22) \quad E_{kin}(t) := \frac{1}{2} \left(\rho_f \|\mathbf{u}\|_{L^2(\Omega_F(t))}^2 + \|\sqrt{\rho_K h} \partial_t \eta\|_{L^2(\Gamma)}^2 \right) \text{ and } E_{el}(t) := \|\eta\|_\gamma + \|\eta\|_\sigma$$

denote the kinetic and elastic energy of the coupled problem, respectively, and the term $D(t)$ captures viscous dissipation in the fluid:

$$(3.23) \quad D(t) := \mu_F \|\mathbf{D}(\mathbf{u})\|_{L^2(\Omega_F(t))}^2.$$

The constant $C(P_{in}(t), P_{out}(t))$ depends only on the inlet and outlet pressure data, which are both functions of time.

The derivation of inequality (3.21) is standard. Details can be found in e.g., [62].

4. WEAK SOLUTIONS

To prove the existence of a weak solution to (3.17)-(3.19) and to design the corresponding numerical solver, we use the so called Arbitrary Lagrangian-Eulerian (ALE) mapping [13, 42, 32, 65] and map the problem onto a fixed domain Ω , which we choose to be a cylinder of radius 1 and length L :

$$\Omega = \{(z, x, y) : z \in (0, L), x^2 + y^2 < 1\}.$$

Mapping onto a fixed domain takes care of problems associated with the moving fluid domain, however,

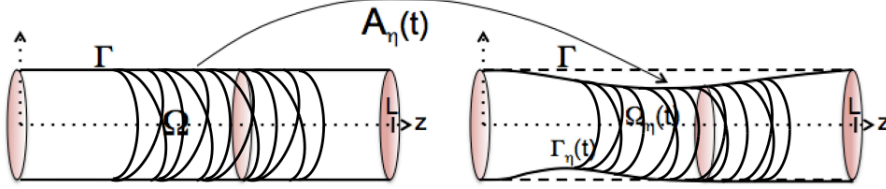


FIGURE 4. ALE mapping.

it also introduces additional nonlinearities into the fluid equations, which we will have to deal with in the existence proof.

4.1. ALE mapping. For each given displacement η , introduce a family of ALE mappings A_η parameterized by η :

$$(4.1) \quad A_\eta(t) : \Omega \rightarrow \Omega_\eta(t), \quad A_\eta(t)(\tilde{z}, \tilde{r}, \tilde{\theta}) := \left(\tilde{z}, (R + \eta(t, \tilde{z}, \tilde{\theta}))\tilde{r}, \tilde{\theta} \right)^T, \quad (\tilde{z}, \tilde{r}, \tilde{\theta}) \in \Omega,$$

where $(\tilde{z}, \tilde{r}, \tilde{\theta})$ denote the cylindrical coordinates in the reference domain Ω . See Figure 4. Since we work with the Navier-Stokes equations written in Cartesian coordinates, it is useful to write an explicit form of the ALE mapping A_η in the Cartesian coordinates as well:

$$(4.2) \quad A_\eta(t)(\tilde{z}, \tilde{x}, \tilde{y}) := \begin{pmatrix} \tilde{z} \\ (R + \eta(t, \tilde{z}, \tilde{\theta}))\tilde{x} \\ (R + \eta(t, \tilde{z}, \tilde{\theta}))\tilde{y} \end{pmatrix}, \quad (\tilde{z}, \tilde{x}, \tilde{y}) \in \Omega.$$

In our numerical simulations, presented in Section 8, the ALE mapping is the harmonic extension of the boundary onto the entire fluid domain.

Mapping $A_\eta(t)$ is a bijection, and its Jacobian is given by

$$(4.3) \quad |\det \nabla A_\eta(t)| = (R + \eta(t, \tilde{z}, \tilde{\theta}))^2.$$

Composite functions with the ALE mapping will be denoted by

$$(4.4) \quad \mathbf{u}^\eta(t, \cdot) = \mathbf{u}(t, \cdot) \circ A_\eta(t) \quad \text{and} \quad p^\eta(t, \cdot) = p(t, \cdot) \circ A_\eta(t).$$

The derivatives of composite functions satisfy:

$$\nabla \mathbf{u} = \nabla \mathbf{u}^\eta (\nabla A_\eta)^{-1} =: \nabla^\eta \mathbf{u}^\eta, \quad \partial_t \mathbf{u} = \partial_t \mathbf{u}^\eta - (\mathbf{w}^\eta \cdot \nabla^\eta) \mathbf{u}^\eta,$$

where the ALE domain velocity, \mathbf{w}^η , is given by:

$$(4.5) \quad \mathbf{w}^\eta = \partial_t \eta(0, \tilde{x}, \tilde{y})^T.$$

The following notation will also be useful:

$$\sigma^\eta = -p^\eta \mathbf{I} + 2\mu \mathbf{D}^\eta(\mathbf{u}^\eta), \quad \mathbf{D}^\eta(\mathbf{u}^\eta) = \frac{1}{2}(\nabla^\eta \mathbf{u}^\eta + (\nabla^\eta)^\tau \mathbf{u}^\eta).$$

First-order system in ALE form. We would like to write system (3.16)-(3.19) in ALE form, which will be convenient to semi-discretize, and to split into a fluid and structure sub-problem by using

an operator splitting strategy. For this purpose we would like to write our problem as a first-order system in time. As in our earlier works [62], we introduce a new variable, v , to denote the trace of the fluid velocity on $\Gamma_\eta(t)$, and replace $\partial_t \eta$ by v in the structure equation by incorporating the kinematic coupling condition (3.12). This way the second-order derivative of η is replaced by the first order derivative of v with respect to time, and the kinematic coupling condition is enforced implicitly everywhere in the formation of the problem. With this, problem (3.16)-(3.17) in ALE form, defined on the reference domain Ω , and written as a first-order system in time, has the following form: *Find $\mathbf{u}^\eta(t, \tilde{z}, \tilde{x}, \tilde{y}), p^\eta(t, \tilde{z}, \tilde{x}, \tilde{y}), \eta(t, \tilde{z}, \tilde{\theta})$, and $v(t, \tilde{z}, \tilde{\theta})$ such that:*

$$(4.6) \quad \left. \begin{aligned} \rho_f (\partial_t \mathbf{u}^\eta + ((\mathbf{u}^\eta - \mathbf{w}^\eta) \cdot \nabla^\eta) \mathbf{u}^\eta) &= \nabla^\eta \cdot \sigma^\eta, \\ \nabla^\eta \cdot \mathbf{u}^\eta &= 0, \end{aligned} \right\} \text{in } (0, T) \times \Omega,$$

$$(4.7) \quad \left. \begin{aligned} p + \frac{\rho_f}{2} |u^\eta|^2 &= P_{in/out}(t), \\ \mathbf{u}^\eta \times \mathbf{e}_z &= 0, \end{aligned} \right\} \text{on } (0, T) \times \Gamma_{in/out},$$

$$(4.8) \quad \left. \begin{aligned} \mathbf{u}^\eta &= v \mathbf{e}_r, \\ \partial_t \eta &= v, \\ \rho_K h \partial_t v + \mathcal{L} \eta &= -J \sigma^\eta \mathbf{n} \cdot \mathbf{e}_r \end{aligned} \right\} \text{on } (0, T) \times (0, L),$$

$$(4.9) \quad \mathbf{u}^\eta(0, \cdot) = \mathbf{u}_0, \eta(0, \cdot) = \eta_0, v(0, \cdot) = v_0, \quad \text{at } t = 0.$$

To simplify notation, in the text that follows, will drop the superscript η in \mathbf{u}^η whenever there is no possibility of confusion.

4.2. Weak formulation. For the fluid velocity we would like to work with the classical function space associated with weak solutions of the Navier-Stokes equations. This, however, requires some additional consideration. Namely, since the fluid domain is also an unknown in the problem, we cannot assume *a priori* any smoothness that is not consistent with the energy estimates, and so the fluid domain boundary may not even be Lipschitz. Indeed, from the energy inequality (3.21) we only have $\eta \in H^2(\omega)$, and from Sobolev embeddings, by taking into account that we are working in \mathbb{R}^3 , we get that $\eta \in C^{0,\mu}(\omega)$, $\mu < 1$. Therefore, the energy estimates imply that $\Omega_\eta(t)$ is not necessarily a Lipschitz domain. However, $\Omega_\eta(t)$ is locally a sub-graph of a Hölder continuous function. In that case one can define the “Lagrangian” trace

$$(4.10) \quad \begin{aligned} \gamma_{\Gamma(t)} &: C^1(\overline{\Omega_\eta(t)}) \rightarrow C(\omega), \\ \gamma_{\Gamma(t)} &: v \mapsto v(t, \tilde{z}, 1 + \eta(t, \tilde{z}, \tilde{\theta}), \tilde{\theta}). \end{aligned}$$

It was shown in [21, 40, 57] that the trace operator $\gamma_{\Gamma(t)}$ can be extended by continuity to a linear operator from $H^1(\Omega_\eta(t))$ to $H^s(\omega)$, $0 \leq s < \frac{1}{2}$. For a precise statement of the results about “Lagrangian” trace see [57]. Now, we can define the velocity solution space defined on the moving domain in the following way:

$$(4.11) \quad \begin{aligned} V_F(t) &= \{ \mathbf{u} = (u_z, u_x, u_y) \in C^1(\overline{\Omega_\eta(t)})^3 : \nabla \cdot \mathbf{u} = 0, \\ &\quad \mathbf{u} \times \mathbf{e}_r = 0 \text{ on } \Gamma(t), \mathbf{u} \times \mathbf{e}_z = 0 \text{ on } \Gamma_{in/out} \}, \\ \mathcal{V}_F(t) &= \overline{V_F(t)}^{H^1(\Omega_\eta(t))}. \end{aligned}$$

Using the fact that $\Omega_\eta(t)$ is locally a sub-graph of a Hölder continuous function we can get the following characterization of the velocity solution space $\mathcal{V}_F(t)$ (see [21, 40]):

$$(4.12) \quad \mathcal{V}_F(t) = \{ \mathbf{u} = (u_z, u_x, u_y) \in H^1(\Omega_\eta(t))^3 : \nabla \cdot \mathbf{u} = 0, \\ \mathbf{u} \times \mathbf{e}_r = 0 \text{ on } \Gamma(t), \mathbf{u} \times \mathbf{e}_z = 0 \text{ on } \Gamma_{in/out} \}.$$

Before defining the fluid velocity space defined on a fixed, reference domain Ω , it is important to point out that the transformed fluid velocity \mathbf{u}^η is not divergence-free anymore. Rather, it satisfies the transformed divergence-free condition $\nabla^\eta \cdot \mathbf{u}^\eta = 0$. Furthermore, since η is not Lipschitz, the ALE

mapping is not necessarily a Lipschitz function either, and, as a result, \mathbf{u}^η is not necessarily in $H^1(\Omega)$. Therefore, we need to redefine the function spaces for the fluid velocity by introducing

$$\mathcal{V}_F^\eta = \{\mathbf{u}^\eta : \mathbf{u} \in \mathcal{V}_F(t)\},$$

where \mathbf{u}^η is defined in (4.4). Under the assumption $R + \eta(t, \tilde{z}, \tilde{\theta}) > 0$, $\tilde{z} \in [0, L]$, we can define a scalar product on \mathcal{V}_F^η in the following way:

$$(\mathbf{u}^\eta, \mathbf{v}^\eta)_{\mathcal{V}_F^\eta} = \int_{\Omega} (R + \eta)^2 (\mathbf{u}^\eta \cdot \mathbf{v}^\eta + \nabla^\eta \mathbf{u}^\eta : \nabla^\eta \mathbf{v}^\eta) = \int_{\Omega_\eta(t)} \mathbf{u} \cdot \mathbf{v} + \nabla \mathbf{u} : \nabla \mathbf{v} = (\mathbf{u}, \mathbf{v})_{H^1(\Omega_\eta(t))}.$$

Therefore, $\mathbf{u} \mapsto \mathbf{u}^\eta$ is an isometric isomorphism between $\mathcal{V}_F(t)$ and \mathcal{V}_F^η , and so \mathcal{V}_F^η is also a Hilbert space.

The function space associated with the Koiter shell equations is standard:

$$\mathcal{V}_K = H_0^2(\omega).$$

From this point on we will be working with the FSI problem mapped via the ALE mapping onto the fixed, reference domain Ω . Motivated by the energy inequality we define the corresponding evolution spaces for the FSI problem defined on Ω :

$$(4.13) \quad \mathcal{W}_F^\eta(0, T) = L^\infty(0, T; L^2(\Omega)) \cap L^2(0, T; \mathcal{V}_F^\eta),$$

$$(4.14) \quad \mathcal{W}_K(0, T) = W^{1, \infty}(0, T; L^2(\omega)) \cap L^2(0, T; H_0^2(\omega)).$$

The corresponding solution and test spaces are defined by:

$$(4.15) \quad \mathcal{W}^\eta(0, T) = \{(\mathbf{u}, \eta) \in \mathcal{W}_F^\eta(0, T) \times \mathcal{W}_K(0, T) : \mathbf{u}|_{r=1} = \partial_t \eta \mathbf{e}_r, \}.$$

$$(4.16) \quad \mathcal{Q}^\eta(0, T) = \{(\mathbf{q}, \psi) \in C_c^1([0, T]; \mathcal{V}_F^\eta \times \mathcal{V}_K) : \mathbf{q}|_{r=1} = \psi \mathbf{e}_r, \}.$$

We will be using b^η to denote the following trilinear form corresponding to the (symmetrized) nonlinear advection term in the Navier-Stokes equations in the fixed, reference domain:

$$(4.17) \quad b^\eta(\mathbf{u}, \mathbf{u}, \mathbf{q}) := \frac{1}{2} \int_{\Omega} (R + \eta)^2 ((\mathbf{u} - \mathbf{w}^\eta) \cdot \nabla^\eta) \mathbf{u} \cdot \mathbf{q} - \frac{1}{2} \int_{\Omega} (R + \eta)^2 ((\mathbf{u} - \mathbf{w}^\eta) \cdot \nabla^\eta) \mathbf{q} \cdot \mathbf{u}.$$

Finally, we define a linear functional which associates the inlet and outlet dynamic pressure boundary data to a test function \mathbf{v} in the following way:

$$\langle F(t), \mathbf{v} \rangle_{\Gamma_{in/out}} = P_{in}(t) \int_{\Gamma_{in}} v_z - P_{out}(t) \int_{\Gamma_{out}} v_z.$$

Definition 4.1. *We say that $(\mathbf{u}, \eta) \in \mathcal{W}^\eta(0, T)$ is a weak solution of problem (4.6)-(4.9) defined on the reference domain Ω , if for every $(\mathbf{q}, \psi) \in \mathcal{Q}^\eta(0, T)$:*

$$(4.18) \quad \begin{aligned} & -\rho_f \left(\int_0^T \int_{\Omega} (R + \eta)^2 \mathbf{u} \cdot \partial_t \mathbf{q} + \int_0^T b^\eta(\mathbf{u}, \mathbf{u}, \mathbf{q}) \right) + 2\mu_F \int_0^T \int_{\Omega} (R + \eta)^2 \mathbf{D}^\eta(\mathbf{u}) : \mathbf{D}^\eta(\mathbf{q}) \\ & -\rho_f \int_0^T \int_{\Omega} (R + \eta) (\partial_t \eta) \mathbf{u} \cdot \mathbf{q} - R \int_0^T \int_{\omega} \rho_K h \partial_t \eta \partial_t \psi + R \int_0^T \int_{\omega} \frac{h}{2} \mathcal{A} \gamma(\eta) : \gamma(\psi) \\ & + R \int_0^T \int_{\omega} \frac{h^3}{24} \mathcal{A} \boldsymbol{\rho}(\eta) : \boldsymbol{\rho}(\psi) = \int_0^T \langle F(t), \mathbf{q} \rangle_{\Gamma_{in/out}} + \int_{\Omega_\eta} (R + \eta_0)^2 \mathbf{u}_0 \cdot \mathbf{q}(0) + \int_{\omega} \varrho_K h v_0 \psi(0). \end{aligned}$$

Here, the coefficients ρ_K, h and the elasticity coefficients in the operator \mathcal{A} are all functions of space and belong to $L^\infty(\omega)$.

This weak formulation is obtained in a standard way by multiplying the PDE by a test function and integrating by parts. The only term that is not standard is the fourth term on the left hand-side of (4.18). This term is obtained from integration by parts of one half of the nonlinear advection term, and it corresponds to the integral $-\rho_f \int_0^T \int_{\Omega} (R + \eta)^2 (\nabla^\eta \cdot \mathbf{w}^\eta) \mathbf{u} \cdot \mathbf{q}$. We calculate

$$\nabla^\eta \cdot \mathbf{w}^\eta = \nabla \cdot \mathbf{w} = \partial_x \left(\partial_t \eta \frac{x}{R + \eta} \right) + \partial_y \left(\partial_t \eta \frac{y}{R + \eta} \right) = x \partial_x \frac{\partial_t \eta}{R + \eta} + y \partial_y \frac{\partial_t \eta}{R + \eta} + 2 \frac{\partial_t \eta}{R + \eta}.$$

Now we notice that for any given function f that depends only on t, z and θ , for example $f = \partial_t \eta / (R + \eta)$, the following holds

$$x \partial_x f + y \partial_y f = \partial_\theta f \frac{-xy}{x^2 + y^2} + \partial_\theta f \frac{xy}{x^2 + y^2} = 0.$$

Thus, we obtain

$$\nabla^\eta \cdot \mathbf{w}^\eta = \nabla \cdot \mathbf{w} = x \partial_x \frac{\partial_t \eta}{R + \eta} + y \partial_y \frac{\partial_t \eta}{R + \eta} + 2 \frac{\partial_t \eta}{R + \eta} = 2 \frac{\partial_t \eta}{R + \eta}.$$

Plugging this expression for $\nabla^\eta \cdot \mathbf{w}^\eta$ into $-\rho_f \int_0^T \int_\Omega (R + \eta)^2 (\nabla^\eta \cdot \mathbf{w}^\eta) \mathbf{u} \cdot \mathbf{q}$ gives the third term in equation (4.18).

5. APPROXIMATE SOLUTIONS

We will prove the existence of a weak solution by proving that a sequence of approximate solutions to our time-splitting numerical scheme converges to a weak solution of the FSI problem. This way we will have also proved that the numerical scheme, based on the time-discretization via operator splitting used in the existence proof, is convergent.

We begin by semi-discretizing problem (4.6)-(4.9) with respect to time. For this purpose let $N \in \mathbb{N}$, introduce the time-discretization step $\Delta t = T/N$, and set $t_n = n\Delta t$. Define approximate solutions on $(0, T)$ to be the functions which are piece-wise constant on each sub-interval $((n-1)\Delta t, n\Delta t]$, $n = 1 \dots N$ of $(0, T)$, such that for $t \in ((n-1)\Delta t, n\Delta t]$, $n = 1 \dots N$,

$$(5.1) \quad \mathbf{X}_N(t, \cdot) = \mathbf{X}_N^n, \quad X_N = (\mathbf{u}_N, v_N, \eta_N),$$

where $\mathbf{X}_N^n = (\mathbf{u}_N^n, v_N^n, \eta_N^n)$, $n = 0, 1, \dots, N$ will be recursively defined by a time-marching operator splitting scheme, which is described below.

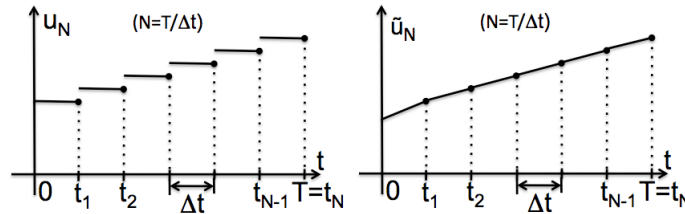


FIGURE 5. A sketch of two different approximations of u_N used in the existence proof: a piece-wise constant approximation u_N (left), and a piece-wise linear approximation \tilde{u}_N (right). The piece-wise constant approximation, shown on the left, is used in the numerical simulations, presented in Section 8.

5.1. An extended Lie splitting strategy. We split the semi-discretized problem (4.6)-(4.9) into a fluid and structure sub-problems by introducing operators A_1 (Structure) and A_2 (Fluid) so that the coupled problem (4.6)-(4.9) can be written as an initial-value problem:

$$\frac{d\phi}{dt} + A\phi = 0 \quad \text{in } (0, T), \quad \phi(0) = \phi_0,$$

where A is an operator defined on a Hilbert space, and A can be written as $A = A_1 + A_2$. The solution of this problem is then found by solving the structure sub-problem, defined by the operator A_1 , over the time interval (t_n, t_{n+1}) , with the initial data given by the solution from the previous time-step, and then solving the fluid sub-problem, defined by the operator A_2 , over the same time interval (t_n, t_{n+1}) , but with the initial data which is equal to the just calculated solution of the problem defined by A_1 [39]. More precisely, the scheme is defined by:

$$\text{Solve } \left\{ \begin{array}{l} \frac{d}{dt} \phi_i + A_i \phi_i = 0 \\ \phi_i(t_n) = \phi^{n+\frac{i-1}{2}} \end{array} \right\} \quad \text{in } (t_n, t_{n+1}), \quad \text{and then set } \phi^{n+\frac{i}{2}} = \phi_i(t_{n+1}), \quad \text{for } i = 1, 2.$$

Following this procedure, for every subdivision of $(0, T)$ containing $N \in \mathbb{N}$ sub-intervals, we recursively define the vector of unknown approximate solutions

$$(5.2) \quad \mathbf{X}_N^{n+\frac{i}{2}} = \left(\mathbf{u}_N^{n+\frac{i}{2}}, v_N^{n+\frac{i}{2}}, \eta_N^{n+\frac{i}{2}} \right)^T, n = 0, 1, \dots, N-1, \quad i = 1, 2,$$

where $i = 1, 2$ denotes the solution of sub-problem A1 or A2, respectively, with the initial condition denoted by:

$$\mathbf{X}^0 = (\mathbf{u}_0, v_0, \eta_0)^T.$$

This is the classical Lie splitting scheme. In the present work, however, we modify this scheme so that the two problems communicate not only through the initial data, but also through the operators A_1 and A_2 . This is new with respect to our earlier works [62, 59] where in our existence proofs we used the splitting in which the sub-problems communicate only via the initial data. The new, extended Lie splitting strategy increases the accuracy of the numerical scheme by lowering the splitting error of the method, as we show numerically in Section 8; see also [15].

The crux of the problem is in constructing the operators A_1 and A_2 such that the resulting scheme is stable and convergent. As we shall see later, this will be accomplished with a splitting that ‘‘preserves’’ the energy inequality (3.21) at the semi-discrete level. We define the semi-discrete version of the kinetic and elastic energy, originally defined in (3.22), and of dissipation, originally defined in (3.23), by the following:

$$(5.3) \quad E_N^{n+\frac{i}{2}} = \frac{1}{2} \left(\rho_f \int_{\Omega} (R + \eta^{n-1+i})^2 |\mathbf{u}_N^{n+\frac{i}{2}}|^2 + \|\sqrt{\rho_K h} v_N^{n+\frac{i}{2}}\|_{L^2(\omega)}^2 \right) + \|\eta_N^{n+\frac{i}{2}}\|_{\gamma}^2 + \|\eta_N^{n+\frac{i}{2}}\|_{\sigma}^2,$$

$$(5.4) \quad D_N^{n+1} = \Delta t \mu_F \int_{\Omega} (R + \eta^n)^2 |D\eta^n(\mathbf{u}_N^{n+1})|^2, \quad n = 0, \dots, N-1, \quad i = 0, 1.$$

The splitting that ‘‘preserves’’ the energy estimate and provides a stable, convergent semi-discrete scheme is based on splitting the dynamic coupling condition:

$$\rho_K h \partial_t v + \mathcal{L}\eta = -J(t, z, \theta)(\boldsymbol{\sigma}\mathbf{n})|_{\Gamma} \cdot \mathbf{e}_r = -(1 - \beta)J(t, z, \theta)(\boldsymbol{\sigma}\mathbf{n})|_{\Gamma} \cdot \mathbf{e}_r - \beta J(t, z, \theta)(\boldsymbol{\sigma}\mathbf{n})|_{\Gamma} \cdot \mathbf{e}_r,$$

into

$$\rho_K h \partial_t v + \mathcal{L}\eta = -\beta J(t, z, \theta)(\boldsymbol{\sigma}\mathbf{n})|_{\Gamma} \cdot \mathbf{e}_r \quad \text{and} \quad \rho_K h \partial_t v = -(1 - \beta)J(t, z, \theta)(\boldsymbol{\sigma}\mathbf{n})|_{\Gamma} \cdot \mathbf{e}_r,$$

and having the condition on the left define the structure sub-problem, and the condition on the right be the boundary condition on Γ for the fluid sub-problem. The parameter β , $0 \leq \beta \leq 1$ distributes the normal stress between the structure and fluid sub-problems. The closer the beta to 1, the more structure loading of the fluid normal stress is felt by the structure, providing a tighter coupling between the fluid and structure sub-problems. This is our extension of the ‘‘classical’’ Lie splitting strategy: the fluid and structure sub-problems communicate not only via the initial data, but also via the loading of the structure by the β -fraction of the normal fluid stress. The crucial point in this splitting is the inclusion of structure inertia in the fluid sub-problem via a Robin-type boundary condition. This is what will make the resulting scheme stable even when the density of the structure is close to the density of the fluid, thereby getting around the difficulties associated with the added mass effect in classical loosely-coupled partitioned schemes [19]. The resulting splitting is the following:

Problem A1 : STRUCTURE

$$\begin{aligned} \partial_t \eta &= v, & \text{on } \Gamma \\ \rho_K h \partial_t v + \mathcal{L}\eta &= -\beta \hat{\boldsymbol{\sigma}}^\eta \mathbf{n}|_{\Gamma} \cdot \mathbf{e}_r, & \text{on } \Gamma \end{aligned}$$

Problem A2 : FLUID in Ω

$$\begin{aligned} \partial_t \mathbf{u} + ((\hat{\mathbf{u}} - \mathbf{w}) \cdot \nabla^\eta) \mathbf{u} &= \nabla^\eta \cdot \boldsymbol{\sigma}^\eta, \\ \nabla^\eta \cdot \mathbf{u} &= 0, \end{aligned}$$

with :

$$\begin{aligned} \mathbf{u}|_{\Gamma} &= v \mathbf{e}_r, \\ \rho_K h \partial_t v + J \boldsymbol{\sigma}^\eta \mathbf{n}|_{\Gamma} \cdot \mathbf{e}_r &= \beta J \hat{\boldsymbol{\sigma}}^\eta \mathbf{n}|_{\Gamma} \cdot \mathbf{e}_r. \end{aligned}$$

Here $\hat{\mathbf{u}}$, $\hat{\boldsymbol{\sigma}}^\eta$ are the values of \mathbf{u} and $\boldsymbol{\sigma}^\eta$ from the previous time step, and \mathbf{w} , which is the domain velocity (the time derivative of the ALE mapping), is obtained from the just calculated Problem A1. Furthermore, ∇^η is the transformed gradient, which is based on the value of η from the previous time-step. The initial data for \mathbf{u} is given from the previous time step, while the initial data for the trace of

the fluid velocity v is given by the just calculated velocity of the thin structure $\partial_t \eta$ in Problem A1. The coefficients h , ρ_K , and E and σ in \mathcal{L} are $L^\infty(\omega)$ -functions.

It was shown in [15] that this approach, with constant h , ρ_K , and the elasticity coefficients E and σ , gives rise to an unconditionally stable partitioned, loosely coupled scheme even when the fluid and structure densities are comparable. No sub-iterations between the sub-problems are needed to achieve stability. In the present manuscript we show that this scheme *converges* to a weak solution of the underlying nonlinear fluid-structure interaction problem, and that this holds even when h , ρ_K , E and σ are functions of space and may allow jump discontinuities to model the presence of a stent.

Weak formulation of the split problem. The above splitting defines two semi-discretized sub-problems, each being a linear problem of elliptic type, for which the existence of a unique solution is guaranteed by the Lax-Milgram Lemma. The weak form of the sub-problems is as follows.

Problem A1: *The structure elastodynamics problem.* We write a semi-discrete version of Problem A1 (Structure Elastodynamics). First we introduce the following notation:

$$(5.5) \quad \sigma^n := \boldsymbol{\sigma}^{\eta^n} \mathbf{n}^{\eta^n} \cdot \mathbf{e}_r,$$

where \mathbf{n}^{η^n} is the unit outer normal on Ω^{η^n} . In this step \mathbf{u} does not change, and so

$$\mathbf{u}^{n+\frac{1}{2}} = \mathbf{u}^n.$$

We define $(v^{n+\frac{1}{2}}, \eta^{n+\frac{1}{2}}) \in H_0^2(\omega) \times H_0^2(\omega)$ as a solution of the following problem, written in weak form:

$$(5.6) \quad \int_{\omega} \frac{\eta^{n+\frac{1}{2}} - \eta^n}{\Delta t} \phi = \int_{\omega} v^{n+\frac{1}{2}} \phi, \quad \forall \phi \in L^2(\omega),$$

$$\int_{\omega} \rho_K h \frac{v^{n+\frac{1}{2}} - v^n}{\Delta t} \psi + \int_{\omega} \frac{h}{2} \mathcal{A} \boldsymbol{\gamma}(\eta^{n+\frac{1}{2}}) : \boldsymbol{\gamma}(\psi) + \int_{\omega} \frac{h^3}{24} \mathcal{A} \boldsymbol{\rho}(\eta^{n+\frac{1}{2}}) : \boldsymbol{\rho}(\psi) = -\beta \int_{\omega} \sigma^n \psi, \quad \forall \psi \in H_0^2(\omega).$$

The first equation is a weak form of the semi-discretized kinematic coupling condition, while the second equation corresponds to a weak form of the semi-discretized elastodynamics equation.

Proposition 5.1. *Let $\lambda, \mu \geq \alpha > 0$ a.e. in ω . For each fixed $\Delta t > 0$, problem (5.6) has a unique solution $(v^{n+\frac{1}{2}}, \eta^{n+\frac{1}{2}}) \in H_0^2(\omega) \times H_0^2(\omega)$.*

Since the Lamé coefficients are such that $\lambda, \mu \geq \alpha > 0$ a.e. in ω , operator \mathcal{A} is coercive. Therefore, the semi-discretized problem is a linear elliptic problem, and so we can use the Lax-Milgram Lemma to show the existence of a unique solution. See [62] for more details.

Proposition 5.2. *For each fixed $\Delta t > 0$, and $h, \rho_K, \lambda, \mu \in L^\infty(\omega)$, solution of problem (5.6) satisfies the following discrete energy equality:*

$$(5.7) \quad E_N^{n+\frac{1}{2}} + \frac{1}{2} \|\sqrt{\rho_K h} (v^{n+\frac{1}{2}} - v^n)\|_{L^2(\omega)}^2 + \|\eta^{n+\frac{1}{2}} - \eta^n\|_{\gamma}^2 + \|\eta^{n+\frac{1}{2}} - \eta^n\|_{\sigma}^2$$

$$= E_N^n - \Delta t \beta \int_{\omega} \sigma^n v^{n+\frac{1}{2}},$$

where the kinetic energy E_N^n is defined in (5.3), and σ^n in (5.5).

The proof is similar to the corresponding proof presented in [62].

Problem A2: *The fluid dynamics problem.* In this step η does not change, and so

$$\eta^{n+1} = \eta^{n+\frac{1}{2}}.$$

Define $(\mathbf{u}^{n+1}, v^{n+1}) \in \mathcal{V}_F^{\eta^n} \times L^2(\omega)$ by requiring that for all $(\mathbf{q}, \psi) \in \mathcal{V}_F^{\eta^n} \times L^2(\omega)$ such that $\mathbf{q}|_\Gamma = \psi \mathbf{e}_r$, the following weak formulation holds:

$$(5.8) \quad \begin{aligned} & \rho_f \int_{\Omega} (R + \eta^n)^2 \left(\frac{\mathbf{u}^{n+1} - \mathbf{u}^{n+\frac{1}{2}}}{\Delta t} \cdot \mathbf{q} + \frac{1}{2} [(\mathbf{u}^n - \mathbf{w}^{n+\frac{1}{2}}) \cdot \nabla \eta^n] \mathbf{u}^{n+1} \cdot \mathbf{q} - \frac{1}{2} [(\mathbf{u}^n - \mathbf{w}^{n+\frac{1}{2}}) \cdot \nabla \eta^n] \mathbf{q} \cdot \mathbf{u}^{n+1} \right) \\ & + \rho_f \int_{\Omega} \left(R + \frac{\eta^n + \eta^{n+1}}{2} \right) v^{n+\frac{1}{2}} \mathbf{u}^{n+1} \cdot \mathbf{q} + 2\mu \int_{\Omega} (R + \eta^n)^2 \mathbf{D}^{\eta^n}(\mathbf{u}) : \mathbf{D}^{\eta^n}(\mathbf{q}) + R \int_{\omega} \rho_K h \frac{v^{n+1} - v^{n+\frac{1}{2}}}{\Delta t} \psi \\ & = \beta \int_{\omega} \sigma^n \psi + R (P_{in}^n \int_0^1 (qz)|_{z=0} - P_{out}^n \int_0^1 (qz)|_{z=L}), \\ & \text{with } \nabla \eta^n \cdot \mathbf{u}^{n+1} = 0, \quad \mathbf{u}|_{\Gamma}^{n+1} = v^{n+1} \mathbf{e}_r, \end{aligned}$$

where $P_{in/out}^n = \frac{1}{\Delta t} \int_{n\Delta t}^{(n+1)\Delta t} P_{in/out}(t) dt$ and $\mathbf{w}^{n+\frac{1}{2}} = v^{n+\frac{1}{2}}(0, \tilde{x}, \tilde{y})^t$.

Notice that this weak formulation was obtained by discretizing the term $-\rho_f \int_0^T \int_{\Omega} (R + \eta)^2 (\nabla \eta \cdot \mathbf{w}^n) \mathbf{u} \cdot \mathbf{q}$ by using

$$\nabla \eta \cdot \mathbf{w}^n = \left(R + \frac{\eta^n + \eta^{n+1}}{2} \right) v^{n+\frac{1}{2}},$$

and by taking into account the kinematic coupling condition $\partial_t \eta = v$. The term $\nabla \eta \cdot \mathbf{w}^n$ measures the change of fluid domain volume due to the motion of the boundary. We chose the particular discretization of the Jacobian of the ALE mapping $(R + \frac{\eta^n + \eta^{n+1}}{2})$ so that the resulting scheme satisfies the geometric conservation law property. See [34] for more details on geometric conservation laws and ALE mappings. This is important for the existence proof, as we shall see later.

Proposition 5.3. *Let $\Delta t > 0$, and assume that η^n are such that $R + \eta^n \geq R_{\min} > 0, n = 0, \dots, N$. Furthermore, assume that the coefficients h and ρ_K are L^∞ functions in ω such that $h, \rho_K \geq \alpha$ a.e. in ω . Then, the fluid sub-problem defined by (5.8) has a unique weak solution $(\mathbf{u}^{n+1}, v^{n+1}) \in \mathcal{V}_F^{\eta^n} \times L^2(\omega)$.*

Proof. Notice again that this is a linear, elliptic problem, and the proof of the existence of a unique solution is obtained by using the Lax-Milgram Lemma. The continuity of the operator is proved by using the Sobolev embedding of $H^1(\Omega)$ into $L^4(\Omega)$. Details of the proof can be found in Proposition 3 in [62]. \square

Proposition 5.4. *For each fixed $\Delta t > 0$, assuming $h, \rho_K \in L^\infty(\omega)$, solution of problem (5.8) satisfies the following discrete energy inequality:*

$$(5.9) \quad \begin{aligned} & E_N^{n+1} + \frac{\rho_f}{2} \int_{\Omega} (R + \eta^n)^2 |\mathbf{u}^{n+1} - \mathbf{u}^n|^2 + \frac{1}{2} \|\sqrt{\rho_K h} (v^{n+1} - v^{n+\frac{1}{2}})\|_{L^2(\omega)}^2 \\ & + D_N^{n+1} \leq \Delta t \beta \int_{\omega} \sigma^n v^{n+1} + E_N^{n+\frac{1}{2}} + C \Delta t ((P_{in}^n)^2 + (P_{out}^n)^2), \end{aligned}$$

where the kinetic energy E_N^n and dissipation D_N^n are defined in (5.3) and (5.4), and the constant C depends only on the parameters in the problem, and not on Δt (or N).

Proof. We begin by focusing on the weak formulation (5.8) in which we replace the test functions \mathbf{q} by \mathbf{u}^{n+1} and ψ by v^{n+1} . We multiply the resulting equation by Δt , and notice that the first term on the right hand-side is given by

$$\frac{\rho_f}{2} \int_{\Omega} (R + \eta^n)^2 |\mathbf{u}^{n+1}|^2.$$

This is the term that contributes to the discrete kinetic energy at the time step $n + 1$, but it does not have the correct form, since the discrete kinetic energy at $n + 1$ is given in terms of the structure location at $n + 1$, and not at n , and so this term should look like:

$$\frac{\rho_f}{2} \int_{\Omega} (R + \eta^{n+1})^2 |\mathbf{u}^{n+1}|^2.$$

To get around this difficulty it is crucial that the advection term is present in the fluid sub-problem. The advection term is responsible for the presence of the integral

$$\rho_f \int_{\Omega} \left(R + \frac{\eta^n + \eta^{n+1}}{2} \right) \Delta t v^{n+\frac{1}{2}} |\mathbf{u}^{n+1}|^2$$

which can be re-written by noticing that $\Delta t v^{n+\frac{1}{2}} := (\eta^{n+1/2} - \eta^n)$ which is equal to $(\eta^{n+1} - \eta^n)$ since, in this sub-problem $\eta^{n+1} = \eta^{n+1/2}$. This implies

$$\frac{\rho f}{2} \left(\int_{\Omega} (R + \eta^n)^2 |\mathbf{u}^{n+1}|^2 + 2 \left(R + \frac{\eta^n + \eta^{n+1}}{2} \right) \Delta t v^{n+\frac{1}{2}} |\mathbf{u}^{n+1}|^2 \right) = \frac{\rho f}{2} \int_{\Omega} (R + \eta^{n+1})^2 |\mathbf{u}^{n+1}|^2.$$

Thus, these two terms combined provide the discrete kinetic energy at the time step $n + 1$. It is interesting to notice how the nonlinearity of the coupling at the deformed boundary requires the presence of nonlinear fluid advection in order for the discrete kinetic energy of the fluid sub-problem to be decreasing in time, and to thus satisfy the desired energy estimate. The rest of the proof is the same as that presented in [62], and is based on the use algebraic identity $(a - b) \cdot a = \frac{1}{2}(|a|^2 + |a - b|^2 - |b|^2)$. \square

Proposition 5.5. *Let $\Delta t > 0$ and let $h, \rho_K, \lambda, \mu \in L^\infty(\omega)$. Furthermore, let $(\eta^{n+1}, v^{n+\frac{1}{2}})$ and (u^{n+1}, v^{n+1}) be solutions of problems (5.6) and (5.8) respectively. Then for each fixed $\beta \in [0, 1]$, the following energy type estimate holds:*

$$(5.10) \quad \begin{aligned} & E_N^{n+1} + \frac{1}{2} \|\sqrt{\rho_K h} (v^{n+\frac{1}{2}} - v^n)\|_{L^2(\omega)}^2 + \|\eta^{n+\frac{1}{2}} - \eta^n\|_{\gamma}^2 + \|\eta^{n+\frac{1}{2}} - \eta^n\|_{\sigma}^2 \\ & + \Delta t^2 \left\| \frac{1}{\sqrt{\rho_K h}} \sigma^{n+1} \right\|_{L^2(\omega)}^2 + \frac{\rho f}{2} \int_{\Omega} (R + \eta^n)^2 |\mathbf{u}^{n+1} - \mathbf{u}^n|^2 + D_N^{n+1} \\ & \leq E_N^n + (\Delta t \beta)^2 \left\| \frac{1}{\sqrt{\rho_K h}} \sigma^n \right\|_{L^2(\omega)}^2 + C \Delta t ((P_{in}^n)^2 + (P_{out}^n)^2). \end{aligned}$$

Proof. First we sum equations (5.7) and (5.9). Since the terms with $E_N^{n+\frac{1}{2}}$ cancel out, we only need to estimate the following term on the right-hand side, which contains β :

$$I = \beta \Delta t \int_{\omega} \sigma^n (v^{n+1} - v^{n+1/2}).$$

Now, from the semi-discretized Robin boundary condition for the fluid sub-problem we get:

$$v^{n+1} - v^{n+\frac{1}{2}} = \frac{\Delta t}{\rho_K h} (\beta \sigma^n - \sigma^{n+1}),$$

and so we can write:

$$\begin{aligned} I &= \Delta t^2 \int_{\omega} \frac{1}{\rho_K h} \frac{1}{2} \left(|\beta \sigma^n|^2 - |\sigma^{n+1}|^2 + |\beta \sigma^n - \sigma^{n+1}|^2 \right) \\ &= \Delta t^2 \frac{1}{2} \left(\beta^2 \left\| \frac{1}{\sqrt{\rho_K h}} \sigma^n \right\|_{L^2(\omega)}^2 - \left\| \frac{1}{\sqrt{\rho_K h}} \sigma^{n+1} \right\|_{L^2(\omega)}^2 \right) + \int_{\omega} \frac{\rho_K h}{2} |v^{n+1} - v^{n+1/2}|^2. \end{aligned}$$

After canceling the last term with the corresponding term on the left-hand side we obtain (5.10). \square

Therefore, we have shown that for each fixed $\Delta t > 0$ the fluid and structure sub-problems, defined on the sub-intervals $(t^n, t^{n+1}), n = 0, \dots, N - 1$, are well-posed, and the solutions of the two sub-problems satisfy energy estimates, which, when combined, give a semi-discrete version of the energy estimate of the continuous problem (3.21). Thus, for each Δt we have designed a time-marching, splitting scheme which defines an approximate solution on $(0, T)$ of our main FSI problem (3.16)-(3.19). The approximate FSI solution satisfies a discrete version of the energy estimate for the continuous problem.

We would like to ultimately show that, as $\Delta t \rightarrow 0$, the sequence of solutions parameterized by N (or Δt), converges to a weak solution of problem (3.16)-(3.19). Furthermore, we also need to show that $R + \eta^n \geq R_{\min} > 0$ is satisfied for each $n = 0, \dots, N - 1$. In order to obtain this result, it is crucial to show that the discrete energy of the sequence of approximate FSI solutions defined for each Δt , is *uniformly bounded*, independently of Δt (or N). This result is obtained by the following Lemma.

Lemma 5.1. (Uniform energy estimates) *Let the parameters $h, \rho_K, \lambda, \mu \in L^\infty(\omega)$ -functions. Let $\Delta t > 0$ be fixed, and $N = T/\Delta t > 0$. Furthermore, let $E_N^{n+\frac{1}{2}}, E_N^{n+1}$, and D_N^j be the kinetic energy and dissipation given by (5.3) and (5.4), respectively, and σ^n be given by (5.5).*

There exists a constant $C > 0$ independent of Δt (and N), which depends only on the parameters in the problem, on the kinetic energy of the initial data E_0 , and on the energy norm of the inlet and outlet data $\|P_{in/out}\|_{L^2(0,T)}^2$, such that the following estimates hold for $0 \leq \beta \leq 1$:

- (1) $E_N^{n+\frac{1}{2}} \leq C, E_N^{n+1} \leq C$, for all $n = 0, \dots, N-1$,
- (2) $\sum_{j=1}^N D_N^j \leq C$,
- (3) $\Delta t^2 \left\| \frac{1}{\sqrt{\rho_K h}} \sigma^n \right\|_{L^2(\omega)}^2 \leq C$,
- (4) $(1 - \beta^2) \Delta t^2 \sum_{n=1}^{N-1} \left\| \frac{1}{\sqrt{\rho_K h}} \sigma^n \right\|_{L^2(\omega)}^2 \leq C$,
- (5) $\sum_{n=0}^{N-1} \left(\int_{\Omega} (R + \eta^n)^2 |\mathbf{u}^{n+1} - \mathbf{u}^n|^2 + \left\| \sqrt{\rho_K h} (v^{n+\frac{1}{2}} - v^n) \right\|_{L^2(\omega)}^2 \right) \leq C$,
- (6) $\sum_{n=0}^{N-1} (\|\eta^{n+1} - \eta^n\|_{\gamma} + \|\eta^{n+1} - \eta^n\|_{\sigma}) \leq C$.
- (7) If $\beta < 1$ we also have $\sum_{n=0}^{N-1} \left\| \sqrt{\rho_K h} (v^{n+1} - v^{n+\frac{1}{2}}) \right\|_{L^2(\omega)}^2 \leq C$.

In fact, $C = E_0 + \tilde{C} \left(\|P_{in}\|_{L^2(0,T)}^2 + \|P_{out}\|_{L^2(0,T)}^2 \right)$, where \tilde{C} is the constant from (5.9), which depends only on the parameters in the problem.

Proof. The proof is similar to the proof of Lemma 1 in [62]. Statements (1)-(6) are directly proved by iterating Proposition 5.5. What remains to show is statement (7). For this purpose we calculate:

$$\sum_{n=0}^{N-1} \left\| \sqrt{\rho_K h} (v^{n+1} - v^{n+\frac{1}{2}}) \right\|_{L^2(\omega)}^2 = \Delta t^2 \sum_{n=0}^{N-1} \left\| \frac{1}{\sqrt{\rho_K h}} (\beta \sigma^n - \sigma^{n+1}) \right\|_{L^2(\omega)}^2.$$

Now the statement follows from the triangle inequality and from statement (4). \square

6. CONVERGENCE OF APPROXIMATE SOLUTIONS

We define approximate solutions of problem (4.6)-(4.9) by combining solutions to the semi-discrete fluid and structure subproblems (5.6) and (5.8), and consider the limit as $\Delta t \rightarrow 0$, i.e., as $N \rightarrow \infty$. We would like to show that the limit as $\Delta t \rightarrow 0$ of approximate solutions is a weak solution of the coupled FSI problem. Uniform estimate will provide weakly and weakly*-convergent subsequences of approximate solutions. To show that the limit satisfies the weak formulation of the continuous FSI problem, weak and weak* convergence will not be sufficient, because of the strong nonlinearities in the coupled FSI problem. To get strong convergence of approximate sub-sequences compactness arguments based on the Simon Lemma [67] will be used, as in our earlier work [58]. Since many of the arguments developed in [58] carry over to the convergence analysis studied in the present manuscript, we summarize the main results, and refer the reader to [58] for more details.

As mentioned earlier in Section 5, we define approximate solutions of problem (4.6)-(4.9) on $(0, T)$ to be the functions which are piece-wise constant on each sub-interval $((n-1)\Delta t, n\Delta t]$, $n = 1 \dots N$ of $(0, T)$, such that for $t \in ((n-1)\Delta t, n\Delta t]$, $n = 1 \dots N$,

$$(6.1) \quad \mathbf{u}_N(t, \cdot) = \mathbf{u}_N^n, \quad \eta_N(t, \cdot) = \eta_N^n, \quad v_N(t, \cdot) = v_N^n, \quad v_N^*(t, \cdot) = v_N^{n-\frac{1}{2}}.$$

See Figure 5 left. Notice that functions $v_N^* = v_N^{n-1/2}$ are determined by Step A1 (the elastodynamics sub-problem), while functions $v_N = v_N^n$ are determined by Step A2 (the fluid sub-problem). As a consequence, functions v_N are equal to the normal trace of the fluid velocity on Γ , i.e., $\mathbf{u}_N = v_N \mathbf{e}_r$. This is not necessarily the case for the functions v_N^* . One can show, however, that the difference between the two sequences converges to zero in L^2 as $\Delta t \rightarrow 0$.

We first show that these approximate sequences are uniformly bounded in the appropriate solutions spaces. The main ingredient in the proof is provided by the uniform estimates from Lemma 5.1. The following Proposition also shows that there exists a $T > 0$ for which $R + \eta_N^n > 0$ holds independently of N and n . This implies, among other things, that our approximate solutions are, indeed, well-defined on a non-zero time interval $(0, T)$.

Proposition 6.1. *Sequence $(\eta_N)_{N \in \mathbb{N}}$ is uniformly bounded in $L^\infty(0, T; H_0^2(\omega))$. Moreover, for T small enough, we have*

$$(6.2) \quad 0 < R_{\min} \leq R + \eta_N(t, z, \theta) \leq R_{\max}, \quad \forall N \in \mathbb{N}, (z, \theta) \in \omega, t \in (0, T).$$

Proof. Uniform boundedness of $(\eta_N)_{N \in \mathbb{N}}$ in $L^\infty(0, T; H_0^2(\omega))$ follows from Lemma 5.1, as in [58]. Using Lemma 5.1 one can also show that $\|\eta_N^n - \eta_0\|_{L^2(\omega)}$ and $\|\eta_N^n - \eta_0\|_{H_0^2(\omega)}$ are both uniformly bounded, see [58]. From the interpolation inequality for Sobolev spaces (see Thrm 4.17 in [2]) we then obtain

$$\|\eta_N^n - \eta_0\|_{H^{3/2}(\omega)} \leq CT^{1/4}, \quad n = 1, \dots, N, \quad N \in \mathbb{N}.$$

From Lemma 5.1 we see that C depends on T through the norms of the inlet and outlet data in such a way that C is an increasing function of T . Therefore by choosing T small, we can make $\|\eta_N^n - \eta_0\|_{H^{3/2}(\omega)}$ arbitrary small for $n = 1, \dots, N, N \in \mathbb{N}$. Because of the Sobolev embedding of $H^{3/2}(\omega)$ into $C(\bar{\omega})$ we can also make $\|\eta_N^n - \eta_0\|_{C(\omega)}$ arbitrarily small. Since the initial data η_0 is such that $R + \eta_0(z, \theta) > 0$ (due to the conditions listed in (3.15)), we see that for a $T > 0$ small enough, there exist $R_{\min}, R_{\max} > 0$, such that

$$0 < R_{\min} \leq R + \eta_N(t, z, \theta) \leq R_{\max}, \quad \forall N \in \mathbb{N}, (z, \theta) \in \omega, t \in (0, T).$$

□

We will show in the end that our existence result holds not only locally in time, i.e., for small $T > 0$, but rather, it can be extended all the way until either $T = \infty$, or until the lateral walls of the channel touch each other.

From this Proposition we see that the L^2 -norm $\|f\|_{L^2(\Omega)}^2 = \int f^2$, and the weighted L^2 -norm $\|f\|_{L^2(\Omega)}^2 = \int (R + \eta_N)^2 f^2$ are equivalent. More precisely, for every $f \in L^2(\Omega)$, there exist constants $C_1, C_2 > 0$, which depend only on R_{\min}, R_{\max} , and not on f or N , such that

$$(6.3) \quad C_1 \int_{\Omega} (R + \eta_N)^2 f^2 \leq \|f\|_{L^2(\Omega)}^2 \leq C_2 \int_{\Omega} (R + \eta_N)^2 f^2.$$

We is used to prove strong convergence of approximate functions.

Next we show that the sequences of approximate solutions for the velocity and its trace on the lateral boundary, are uniformly bounded. To do that, we introduce the following notation which will be useful in the remainder of this manuscript to prove compactness: denote by τ_h the translation in time by h of function f , namely:

$$(6.4) \quad \tau_h f(t, \cdot) = f(t - h, \cdot), \quad h \in \mathbb{R}.$$

By using Lemma 5.1, and the fact that $(v_N)_{n \in \mathbb{N}}, (v_N^*)_{n \in \mathbb{N}}$ and $(\mathbf{u}_N)_{n \in \mathbb{N}}$ as all step-functions in t , one can easily show that the following uniform bounds hold:

Proposition 6.2. *The following statements hold:*

- (1) $(v_N)_{n \in \mathbb{N}}$ is uniformly bounded in $L^\infty(0, T; L^2(\omega))$.
- (2) $(v_N^*)_{n \in \mathbb{N}}$ is uniformly bounded in $L^\infty(0, T; L^2(\omega))$.
- (3) $(\mathbf{u}_N)_{n \in \mathbb{N}}$ is uniformly bounded in $L^\infty(0, T; L^2(\Omega))$.
- (4) $(\mathbf{D}^{\tau_{\Delta t} \eta_N}(\mathbf{u}_N))_{n \in \mathbb{N}}$ is uniformly bounded in $L^2((0, T) \times \Omega)$.

Unfortunately, having the boundedness of the symmetrized gradient is not sufficient to show that the approximate solutions converge to a weak solution of the coupled FSI problem. We need be able to control the behavior of the gradient itself. For this purpose, we can use the following Proposition, proved in [58]:

Proposition 6.3. *The gradient $(\nabla^{\tau_{\Delta t} \eta_N}(\mathbf{u}_N))_{n \in \mathbb{N}}$ is uniformly bounded in $L^2((0, T) \times \Omega)$.*

From the uniform boundedness of approximate sequences we can now conclude that for each approximate solution sequence there exists a subsequence which, with a slight abuse of notation, we denote the same way as the original sequence, and which converges weakly, or weakly*, depending on the function space. More precisely, we have the following result.

Lemma 6.1. (Weak and weak* convergence results) *There exist subsequences $(\eta_N)_{N \in \mathbb{N}}$, $(v_N)_{N \in \mathbb{N}}$, $(v_N^*)_{N \in \mathbb{N}}$, and $(\mathbf{u}_N)_{N \in \mathbb{N}}$, and the functions $\eta \in L^\infty(0, T; H_0^2(\omega))$, $v \in L^\infty(0, T; L^2(\omega)) \cap L^2(0, T; H_0^2(\omega))$, $v^* \in L^\infty(0, T; L^2(\omega))$, and $\mathbf{u} \in L^\infty(0, T; L^2(\Omega))$, such that*

$$(6.5) \quad \begin{aligned} \eta_N &\rightharpoonup \eta \text{ weakly* in } L^\infty(0, T; H_0^2(\omega)), \\ v_N &\rightharpoonup v \text{ weakly in } L^2(0, T; L^2(\omega)), \\ v_N &\rightharpoonup v \text{ weakly* in } L^\infty(0, T; L^2(\omega)), \\ v_N^* &\rightharpoonup v^* \text{ weakly* in } L^\infty(0, T; L^2(\omega)), \\ \mathbf{u}_N &\rightharpoonup \mathbf{u} \text{ weakly* in } L^\infty(0, T; L^2(\Omega)), \\ \nabla^{\tau \Delta t \eta_N} \mathbf{u}_N &\rightharpoonup \mathbf{G} \text{ weakly in } L^2((0, T) \times \Omega). \end{aligned}$$

Furthermore,

$$(6.6) \quad v = v^*.$$

Proof. The only thing left to show is that $v = v^*$. To show this, we multiply statement (3) in Lemma 5.1 by Δt , and notice again that $\|v_N\|_{L^2((0, T) \times \omega)}^2 = \Delta t \sum_{n=1}^N \|v_N^n\|_{L^2(\omega)}^2$. This implies $\|v_N - v_N^*\|_{L^2((0, T) \times \omega)}^2 = \Delta t \sum_{n=1}^N |v_N^n - v_N^{n-\frac{1}{2}}|^2 \leq C \Delta t$, and we have that in the limit, as $\Delta t \rightarrow 0$, $v = v^*$. \square

We would like to prove that the limit $\mathbf{G} = \nabla \eta \mathbf{u}$, where η is the limiting displacement determining the fluid-structure interface location. However, to achieve this goal we will need some stronger convergence properties of approximate solutions. Therefore, we postpone the proof until Proposition 7.1.

6.1. Strong convergence of approximate sequences. To show that the limits obtained in the previous Lemma satisfy the weak form of problem (4.6)-(4.9), we need to show that our sequences converge strongly in the appropriate function spaces. For this purpose, as in [58], we use Simon's compactness theorem which characterizes compact sets in $L^p(0, T; X)$, where X is a Banach space [67]. Simon's theorem says that for a set F , $F \hookrightarrow L^p(0, T; X)$, with $1 \leq p < \infty$ to be relatively compact in $L^p(0, T; X)$, it is necessary and sufficient that the following two properties are satisfied:

- (i) $\|\tau_h f - f\|_{L^p(h, T; X)} \rightarrow 0$ as h goes to zero, uniformly in $f \in F$ (integral "equicontinuity" in time), and
- (ii) $\left\{ \int_{t_1}^{t_2} f(t) dt : f \in F \right\}$ is relatively compact in X , $0 < t_1 < t_2 < T$ (spatial compactness).

Simon's compactness theorem implies compactness of the weakly convergence sub-sequences for the fluid and structure velocities. More precisely, we have the following result.

Theorem 6.1. *For each fixed β , $0 \leq \beta < 1$, sequences $(v_N)_{N \in \mathbb{N}}$, $(\mathbf{u}_N)_{N \in \mathbb{N}}$ are relatively compact in $L^2(0, T; L^2(\omega))$ and $L^2(0, T; L^2(\Omega))$ respectively.*

Proof. The proof of this theorem is the same as the proof of Theorem 5.1 in [58] except for the part related to proving the "integral equicontinuity" property of $(v_N)_{N \in \mathbb{N}}$, i.e., estimate (i) from Simon's theorem. It is here that we must use statement (7) from Lemma 5.1, which holds for $0 \leq \beta < 1$, to obtain

$$(6.7) \quad \|\sqrt{\rho_K h}(\tau_h v_N - v_N)\|_{L^2((0, T) \times \omega)} \rightarrow 0, \quad h \rightarrow 0, \text{ uniformly } \in N.$$

We note that in Theorem 5.1 in [58], the compactness results for the fluid and structure velocities hold for $\beta = 0$, i.e., for the classical Lie splitting strategy, in which case uniform energy estimates of the semi-discrete sub-problems imply uniform boundedness of $\sum_{n=0}^{N-1} \|v^{n+1} - v^{n+1/2}\|_{L^2(\omega)}^2$ and $\sum_{n=0}^{N-1} \|v^{n+1/2} - v^n\|_{L^2(\omega)}^2$, which is used in the compactness proof for the structure velocity. In the case when $0 < \beta < 1$, i.e., in the new, extended Lie splitting strategy discussed in the present manuscript, we use statement (7) of Lemma 5.1 to conclude uniform boundedness of $\sum_{n=0}^{N-1} \|\sqrt{\rho_K h}(v^{n+1} - v^{n+1/2})\|_{L^2(\omega)}^2$. The rest of the proof of Theorem 6.1 follows the same ideas as the proof of Theorem 5.1 in [58]. \square

To show compactness of $(\eta_N)_{N \in \mathbb{N}}$ we introduce a slightly different set of approximate functions of \mathbf{u} , v , and η . Namely, for each fixed Δt (or $N \in \mathbb{N}$), define $\tilde{\mathbf{u}}_N$, $\tilde{\eta}_N$ and \tilde{v}_N to be continuous, linear on

each sub-interval $[(n-1)\Delta t, n\Delta t]$, and such that

$$(6.8) \quad \tilde{\mathbf{u}}_N(n\Delta t, \cdot) = \mathbf{u}_N(n\Delta t, \cdot), \quad \tilde{v}_N(n\Delta t, \cdot) = v_N(n\Delta t, \cdot), \quad \tilde{\eta}_N(n\Delta t, \cdot) = \eta_N(n\Delta t, \cdot),$$

where $n = 0, \dots, N$. See Figure 5 right. Using the same approaches as in [62], Section 6, we can show the following strong convergence results:

Theorem 6.2. *There exist subsequences $(\eta_N)_{N \in \mathbb{N}}, (v_N)_{N \in \mathbb{N}}$, such that*

$$(6.9) \quad \begin{aligned} v_N &\rightarrow v \text{ in } L^2(0, T; L^2(\omega)), \\ \tau_{\Delta t} \mathbf{u}_N &\rightarrow \mathbf{u} \text{ in } L^2(0, T; L^2(\Omega)), \\ \tau_{\Delta t} v_N &\rightarrow v \text{ in } L^2(0, T; L^2(\omega)), \\ \eta_N &\rightarrow \eta \text{ in } L^\infty(0, T; H_0^s(\omega)), \quad s < 2 \\ \tau_{\Delta t} \eta_N &\rightarrow \eta \text{ in } L^\infty(0, T; H_0^s(\omega)), \quad s < 2 \\ \tilde{\mathbf{u}}_N &\rightarrow \mathbf{u} \text{ in } L^2(0, T; L^2(\Omega)), \\ \tilde{v}_N &\rightarrow v \text{ in } L^2(0, T; L^2(0, L)). \end{aligned}$$

From the Sobolev embedding $H^s(\omega)$ into $C(\bar{\omega})$, $s > 1$, we get the following strong convergence results for the approximations of the fluid-structure interface Γ .

Corollary 6.1.

$$(6.10) \quad \begin{aligned} \eta_N &\rightarrow \eta \text{ in } L^\infty(0, T; C(\omega)), \\ \tau_{\Delta t} \eta_N &\rightarrow \eta \text{ in } L^\infty(0, T; C(\omega)). \end{aligned}$$

By using these strong convergence results we will be able to pass to the limit as $N \rightarrow \infty$ in the weak form of the semi-discretized FSI problem, and show that the strong limits satisfy the weak form of the continuous FSI problem, namely, that they are the weak solutions of problem (4.6)-(4.9).

7. THE LIMITING PROBLEM

Before we can show that the limiting functions satisfy the weak form (4.18) of problem (4.6)-(4.9) we must observe that, unfortunately, the velocity test functions in (5.8) depend on N . More precisely, they depend on η_N^n because of the requirement that the transformed divergence-free condition $\nabla^{\eta_N^n} \cdot \mathbf{q} = 0$ must be satisfied. This is a consequence of the fact that we mapped our problem onto a fixed domain Ω . Therefore we will need to take special care in constructing the suitable velocity test functions so that we can pass to the limit in (5.8). In the case of Cartesian coordinates, it was shown in [62], Section 7 (see also [59, 21, 58]) that there exists a set of test function $\mathcal{X}^\eta(0, T)$ which is dense in $\mathcal{Q}^\eta(0, T)$, where the test functions are independent of N , and are well approximated by the test functions \mathbf{q}_N . In cylindrical coordinates there is an additional technical difficulty coming from the fact that extensions by a constant of the functions defined on the interface are not divergence free as in the case of Cartesian coordinates. However, one can use the lifting operator constructed in [53] (Proposition 2.19) instead of the constant extension and analogously, as in [62], Section 7, construct a subset $\mathcal{X}^\eta(0, T)$ with the following properties:

- $\mathcal{X}^\eta(0, T)$ is dense in $\mathcal{Q}^\eta(0, T)$,
- For every $(\mathbf{q}, \psi) \in \mathcal{X}^\eta(0, T)$ there exists a $N_q \in \mathbb{N}$ and a sequence $(\mathbf{q}_N)_{N \geq N_q}$ such that $\mathbf{q}_N \in \mathcal{W}_F^{\tau_{\Delta t} \eta_N}(0, T)$, and
 - (1) $\mathbf{q}_N \rightarrow \mathbf{q}$ uniformly on $[0, T] \times \Omega$;
 - (2) $\nabla^{\tau_{\Delta t} \eta_N}(\mathbf{q}_N) \rightarrow \nabla^\eta(\mathbf{q})$ in $L^2((0, T) \times \omega)$.

The last thing we need to do before we pass to the limit in the weak formulation of the coupled FSI problem is to show that the gradients of the approximate velocities converge to the gradient of the limiting velocity, namely, it remains to identify the function \mathbf{G} introduced in Lemma 6.1. We have the following result:

Proposition 7.1. $\mathbf{G} = \nabla^\eta \mathbf{u}$, where \mathbf{G} , \mathbf{u} and η are the weak and weak* limits given by Lemma 6.1.

Proof. The proof is analogous to the proof of Proposition 7.6. in [59], and it relies on the following main ingredients:

- Uniform convergence of the sequence $\tau_{\Delta t} \eta_N$ which is given by Corollary 6.1; and

- The proof uses the approximate fluid velocities and the limiting fluid velocity transformed back onto the physical domains:

$$\mathbf{u}^N(t, \cdot) = \mathbf{u}_N(t, \cdot) \circ A_{\tau_{\Delta t} \eta_N}^{-1}(t), \quad \tilde{\mathbf{u}}(t, \cdot) = \mathbf{u}(t, \cdot) \circ A_{\eta}^{-1}(t),$$

as well as the fact that $\nabla \mathbf{u}^N = \nabla^{\tau_{\Delta t} \eta_N} \mathbf{u}_N$ and $\nabla \tilde{\mathbf{u}} = \nabla^{\eta} \mathbf{u}$.

Both of these are satisfied in the present case. Since the proof is rather technical we omit the details here and refer the reader to [59]. \square

To get to the weak formulation of the coupled problem, take the test functions $(\mathbf{q}_N(t), \psi(t))$ (where \mathbf{q}_N is a sequence of test function corresponding to $(\mathbf{q}, \psi) \in \mathcal{X}^{\eta}$) in equation (5.8) and integrate with respect to t from $n\Delta t$ to $(n+1)\Delta t$. Furthermore, take $\psi(t)$ as the test functions in (5.6), and again integrate over the same time interval. Add the two equations together, and notice that the terms containing $\beta \in [0, 1)$ cancel out. We then take the sum from $n = 0, \dots, N-1$ to get to the time integrals over $(0, T)$ and obtain the following:

$$(7.1) \quad \begin{aligned} & \rho_f \int_0^T \int_{\Omega} (R + \tau_{\Delta t} \eta_N)^2 \left(\partial_t \tilde{\mathbf{u}}_N \cdot \mathbf{q}_N + \frac{1}{2} (\tau_{\Delta t} \mathbf{u}_N - \mathbf{w}_N) \cdot \nabla^{\tau_{\Delta t} \eta_N} \mathbf{u}_N \cdot \mathbf{q}_N \right. \\ & \left. - \frac{1}{2} (\tau_{\Delta t} \mathbf{u}_N - \mathbf{w}_N) \cdot \nabla^{\tau_{\Delta t} \eta_N} \mathbf{q}_N \cdot \mathbf{u}_N \right) + \rho_f \int_0^T \left(R + \frac{1}{2} (\tau_{\Delta t} \eta_N + \eta_N) \right) \int_{\Omega} v_N^* \mathbf{u}_N \cdot \mathbf{q}_N \\ & + \int_0^T \int_{\Omega} (R + \tau_{\Delta t} \eta_N)^2 2\mu_F \mathbf{D}^{\tau_{\Delta t} \eta_N}(\mathbf{u}_N) : \mathbf{D}^{\tau_{\Delta t} \eta_N}(\mathbf{q}_N) + \int_0^T \int_{\omega} \rho_K h \partial_t \tilde{v}_N \psi R \\ & + \int_0^T \int_{\omega} \frac{h}{2} \mathcal{A} \boldsymbol{\gamma}(\eta) : \boldsymbol{\gamma}(\psi) R + \int_0^T \int_{\omega} \frac{h^3}{24} \mathcal{A} \boldsymbol{\rho}(\eta) : \boldsymbol{\rho}(\psi) R \\ & = \left(\int_0^T P_{in}^N dt \int_0^1 q_z(t, 0, r) R dr - \int_0^T P_{out}^N dt \int_0^1 q_z(t, L, r) R dr \right), \end{aligned}$$

with

$$(7.2) \quad \begin{aligned} & \nabla^{\tau_{\Delta t} \eta} \cdot \mathbf{u}_N = 0, \quad v_N = ((u_r)_N)|_{\Gamma}, \\ & \mathbf{u}_N(0, \cdot) = \mathbf{u}_0, \quad \eta(0, \cdot)_N = \eta_0, \quad v_N(0, \cdot) = v_0. \end{aligned}$$

Here $\tilde{\mathbf{u}}_N$ and \tilde{v}_N are the piecewise linear functions defined in (6.8), $\tau_{\Delta t}$ is the shift in time by Δt to the left, defined in (6.4), $\nabla^{\tau_{\Delta t} \eta_N}$ is the transformed gradient via the ALE mapping $A_{\tau_{\Delta t} \eta_N}$, defined in (4.5), and v_N^* , \mathbf{u}_N , v_N and η_N are defined in (6.1).

Now we can use the convergence results from Proposition 6.1, Theorem 6.2, Lemma 6.5 and Corollary 6.1, and arguments analogous to those in [62], to pass to the limit in (7.2) to obtain the following main result:

Theorem 7.1. *Let ρ_f , ρ_K , μ_F , h , μ , λ be $L^\infty(\omega)$ -functions that are all bounded away from zero. Suppose that the initial data $v_0 \in L^2(\omega)$, $\mathbf{u}_0 \in L^2(\Omega_{\eta_0})$, and $\eta_0 \in H_0^2(\omega)$ are such that $(R + \eta_0(z, \theta)) > 0$, $(z, \theta) \in \omega$. Furthermore, let $P_{in}, P_{out} \in L_{loc}^2(0, \infty)$.*

Then there exist a $T > 0$ and a weak solution (\mathbf{u}, η) of problem (3.16)-(3.19) on $(0, T)$ in the sense of Definition 4.1, which satisfies the following energy estimate:

$$(7.3) \quad E(t) + \int_0^t D(\tau) d\tau \leq E_0 + C(\|P_{in}\|_{L^2(0,t)}^2 + \|P_{out}\|_{L^2(0,t)}^2), \quad t \in [0, T],$$

where C depends only on the coefficients in the problem, E_0 is the kinetic energy of initial data, and $E(t)$ and $D(t)$ are given by

$$\begin{aligned} E(t) &= \frac{\rho_f}{2} \|\mathbf{u}\|_{L^2(\Omega_{\eta(t)})}^2 + \frac{1}{2} \|\sqrt{\rho_K h} \partial_t \eta\|_{L^2(\omega)}^2 + \|\eta\|_{\gamma}^2 + \|\eta\|_{\sigma}^2, \\ D(t) &= \mu_F \|\mathbf{D}(\mathbf{u})\|_{L^2(\Omega_{\eta(t)})}^2, \end{aligned}$$

where

$$\|f\|_{\gamma} := \int_{\omega} \frac{h}{4} \mathcal{A} \boldsymbol{\gamma}(f) : \boldsymbol{\gamma}(f) R, \quad \|f\|_{\sigma} := \int_{\omega} \frac{h^3}{48} \mathcal{A} \boldsymbol{\sigma}(f) : \boldsymbol{\sigma}(f) R,$$

are the energy norms defined by the membrane and flexural effects of the linearly elastic Koiter shell, where the elasticity operator \mathcal{L} is defined in (3.4). They are equivalent to the standard $L^2(\omega)$ and $H_0^2(\omega)$ norms, respectively.

Furthermore, one of the following is true: either

- (1) $T = \infty$, or
- (2) $\lim_{t \rightarrow T} \min_{z \in [0, L]} (R + \eta(z)) = 0$.

Proof. It only remains to prove the last assertion, which states that our result is either global in time, or, in case the walls of the cylinder touch each other, our existence result holds until the time of touching. However, the proof of this argument follows the same reasoning as the proof of the Main Theorem in [62], and the proof of the main result in [21], p. 397-398. We avoid repeating those arguments here, and refer the reader to references [62, 21]. \square

8. NUMERICAL SIMULATIONS

We implemented the extended Lie splitting strategy, described in Section 5.1, into a numerical solver, and studied the performance of three different stent configurations on the solution of the corresponding FSI problem. The cylindrical Koiter shell model (3.8) was considered, with the reference configuration Γ corresponding to the cylinder of constant radius $R = 0.5$ cm and length $L = 5$ cm. All the structure parameters are assumed to be piecewise constant functions on ω , with the values that are higher in the region where the stent is located. We have used the following well-known relationships between the Lamé constants of elasticity and the Youngs modulus E and Poisson ratio σ :

$$\frac{2\mu\lambda}{\lambda + 2\mu} + 2\mu = 4\mu \frac{\lambda + \mu}{\lambda + 2\mu} = \frac{E}{1 - \sigma^2}, \quad \frac{2\mu\lambda}{\lambda + 2\mu} = 4\mu \frac{\lambda + \mu}{\lambda + 2\mu} \frac{1}{2} \frac{\lambda}{\lambda + \mu} = \frac{E}{1 - \sigma^2} \sigma,$$

to express our operator \mathcal{L} in terms of $E = E(z, \theta)$ and $\sigma = \sigma(z, \theta)$. The values of E and σ are given in Table 1 left, with the fluid viscosity μ_F and fluid density ρ_f given in Table 1 right:

	$E[\text{dyne}/\text{cm}^2]$	σ	$h[\text{cm}]$	$\rho_K[\text{g}/\text{cm}^3]$
Artery	10^6	0.5	0.01	1.1
Stent	2.4×10^{12}	0.31	0.1	8.5

	$\mu_F[\text{g}/\text{cms}]$	$\rho_f[\text{g}/\text{cm}^3]$
Fluid	0.035	1

TABLE 1. Parameter values: structure (table on the left) and fluid (table on the right).

Although the existence proof was presented for the case when only the radial component of displacement was assumed to be different from zero, the numerical simulations were performed for the cylindrical Koiter shell model allowing both radial and longitudinal displacements to be different from zero. Furthermore, in the simulations we consider the initial, reference configuration to be axially symmetric and the inlet and outlet data (fluid loading) to be axially symmetric as well. Thus, we expect to have an axially symmetric solution, which implies that nothing in the operator \mathcal{L} , defined in (3.7), depends on the azimuthal variable θ . With the model parameters presented in Table 1, the leading order behavior of the model given in (3.8) captures only the membrane effects. However, we are free to add the “lower order terms” (i.e., the terms of order ϵ^2 or smaller, where $\epsilon = R/L$) to capture the leading-order bending rigidity effects. These terms will contribute to the modeling of wave propagation phenomena in arterial walls, since the resulting structure model takes the form of a linear wave equation (with L^∞ coefficients) for the axial and radial components of displacement η_z and η_r . Written in weak form the model reads:

$$(8.1) \quad \int_0^{2\pi} \int_0^L \rho_K h \partial_t^2 \eta_z \psi_z dz d\theta + \int_0^{2\pi} \int_0^L C_1 \frac{\partial \eta_z}{\partial z} \frac{\partial \psi_z}{\partial z} dz d\theta = \int_0^{2\pi} \int_0^L f_z \psi_z dz d\theta, \quad \forall \psi_z \in H_0^2(\omega),$$

$$\int_0^{2\pi} \int_0^L \rho_K h \partial_t^2 \eta_r \psi_r dz d\theta + \int_0^{2\pi} \int_0^L \left(C_0 \eta_r \psi_r + C_2 \frac{\partial \eta_r}{\partial z} \frac{\partial \psi_r}{\partial z} \right) dz d\theta = \int_0^{2\pi} \int_0^L f_r \psi_r dz d\theta, \quad \forall \psi_r \in H_0^2(\omega),$$

where

$$(8.2) \quad C_0 = \frac{hE}{R^2(1-\sigma^2)}, \quad C_1 = \frac{h^3E\sigma}{6R^2(1-\sigma^2)}, \quad C_2 = \frac{hE}{1-\sigma^2}$$

are all piecewise constant functions of (z, θ) . In (8.1) the term containing C_0 captures membrane effects, while the terms containing C_1 and C_2 capture bending rigidity, i.e. leading-order shell effects. The flow is driven by the time-dependent pressure data:

$$(8.3) \quad p_{in}(t) = \begin{cases} \frac{p_{max}}{2} \left(1 - \cos\left(\frac{2\pi t}{t_{max}}\right)\right) & \text{it } t \leq t_{max}, \\ 0 & \text{it } t > t_{max}, \end{cases} \quad p_{out}(t) = 0, \quad \forall t \in (0, T),$$

where $p_{max} = 1.333 \cdot 10^4$ dyne/cm² and $t_{max} = 5$ ms. All the examples presented below are solved over the time interval $[0, 12]$ ms. The values of the parameters used in all the examples are given in Table 1. In all the simulations we used the value of the splitting parameter $\beta = 1$, except in the last example where we compared the accuracy of the scheme with $\beta = 0$ and $\beta = 1$. We assumed that all the stents we consider have the same mechanical properties, and only differ in the geometric distribution of the stent struts. See Figure 6.

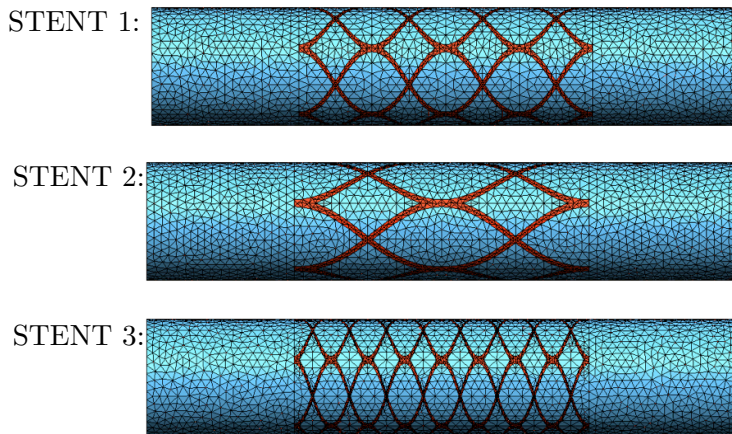


FIGURE 6. The three stent configurations (with computational mesh) considered in this study.

Our splitting algorithm was implemented in a Finite Element Method solver provided in FreeFem++ [1]. For all three stent configurations, the fluid domain consists of approximately 18000 nodes and 100,000 tetrahedral elements. The time step is $\Delta t = 10^{-4}$.

Thus, we study the fluid velocity, pressure, and displacement of the arterial wall treated with a stent, during the time interval $[0, 12]$ ms after the pressure pulse in the form of a shifted cosine function, given by (8.3), hits the inlet of the cylindrical tube. The stents that we consider have strut distribution of medium (Stent 1), low (Stent 2) and high density (Stent 3), as shown in Figure 6.

In all three cases we see that the inlet pressure pulse generates a wave that inflates the cylindrical tube (arterial wall) near the inlet, travels through the stent, and hits the outlet of the tube. Figures 7, 8, and 9 show magnified displacement (left panel) and velocity (right panel) at three different times $t = 2, 4, 7$ ms, for Stent 1, 2, and 3, respectively. In all three figures one can clearly see that the presence of a stent generates a reflected wave at the proximal site of the prosthesis (i.e., at the inlet of the stent). More precisely, the wave with a positive amplitude (the inflated tube), traveling from left to right, shown in all the figures at times $t = 2$ and $t = 4$ ms, hits the stent at around $t = 4$ ms, and a part of the incident wave gets transmitted through the stent, while a large part gets reflected with a negative amplitude, traveling backwards upstream along the arterial wall, shown at $t = 7$ ms. We see that at $t = 7$ ms the reflected wave produces changes not only in the cylinder (arterial) wall, but also in the fluid (blood) velocity. One can see in all the panels on the right, that at times $t = 4$ and $t = 7$ ms the fluid velocity dips significantly near the proximal site of the stent (the blue region indicating zero velocity),

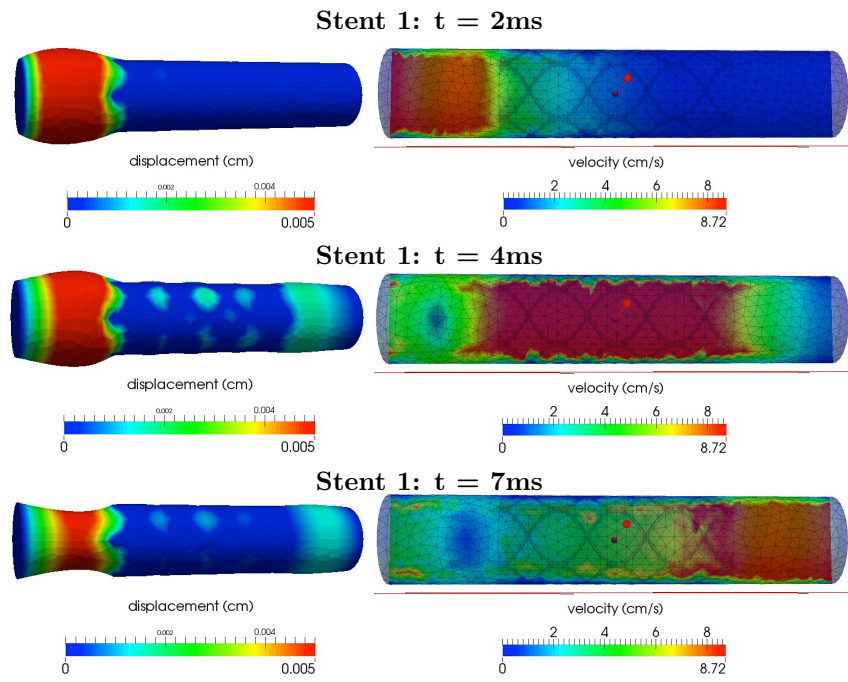


FIGURE 7. Stent 1 at $t = 2, 4$ and 7 ms. Left: Magnified displacement (50x); Right: Velocity.

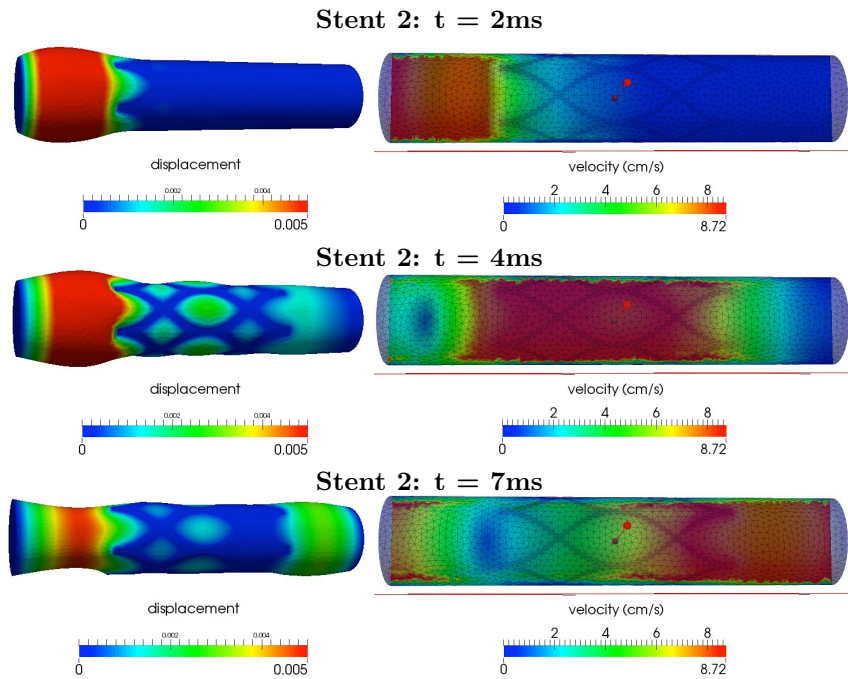


FIGURE 8. Stent 2 at $t = 2, 4$ and 7 ms. Left: Magnified displacement (50x); Right: Velocity.

which induces significant disturbance in fluid (blood) flow near the proximal site of the prosthesis. This may have significant consequences for the physiology and pathophysiology of the arterial wall, and for the local and global blood flow patterns in patients treated with a stent.

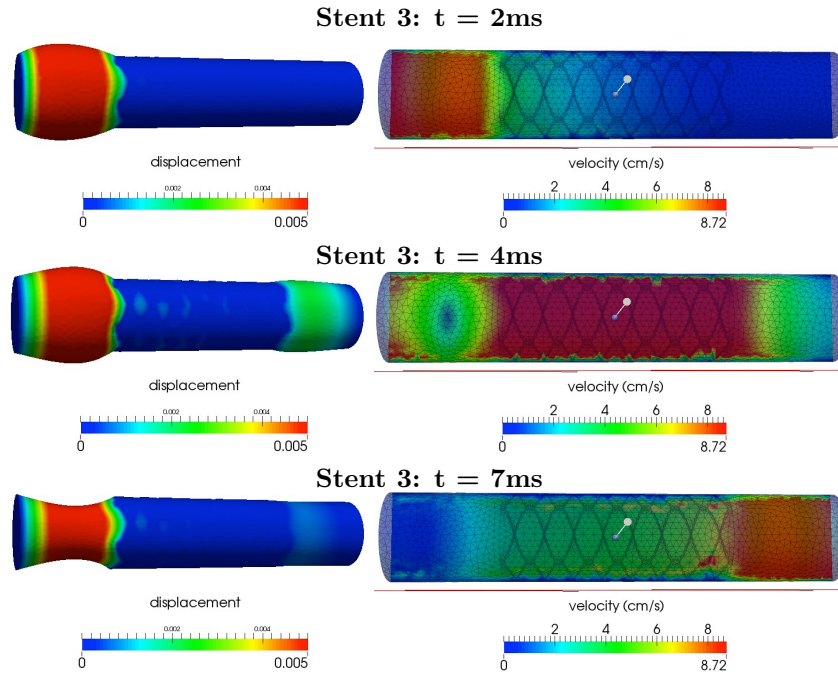


FIGURE 9. Stent 3 at $t = 2, 4$ and 7 ms. Left: Magnified displacement (50x); Right: Velocity.

We compared the difference in the displacement between the three different stent configurations. Due to their stent strut distribution Stent 1 has medium overall rigidity, Stent 2 is the softest of the three, and Stent 3 is the most rigid [68, 18]. The stent strut distribution, and therefore the overall, global stent stiffness, influences the amount of energy that is absorbed by each stent at the moment when the pressure pulse hits the stent at the proximal site (i.e., from the left). Indeed, Figure 10, $t = 7$ ms,

Three stents comparison in magnitude of displacement at $t = 2, 4, 7$ ms

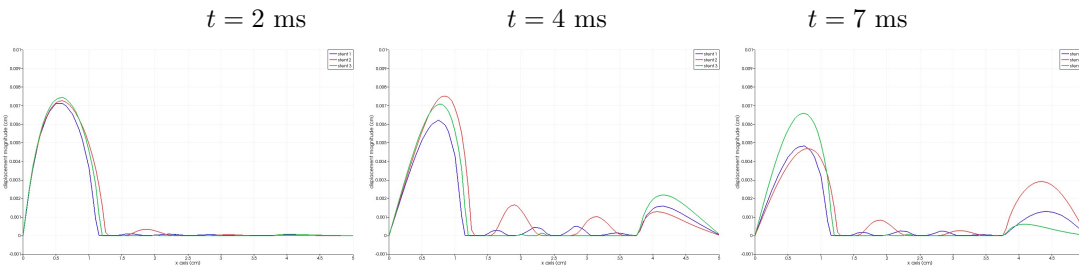


FIGURE 10. Comparison between stents 1, 2, and 3 in magnitude of displacement at $t = 2, 4, 7$ ms. The horizontal axis is the z -axis of the cylinder. The vertical axis is the magnitude of displacement. Displacement of Stent 1 is shown in blue line, Stent 2 in red line, and Stent 3 in green line.

shows that the softest stent absorbs the largest amount of energy, producing a reflected wave with the smallest amplitude, while the stiffest stent produces the reflected wave with the largest amplitude. More precisely, the three panels in Figure 10 show the magnitude of displacement at times $t = 2, 4, 7$ ms, for Stent 1, 2, and 3. The magnitudes of displacement are superimposed for the three stents, and are shown in blue line for Stent 1, in red line for Stent 2, and in green line for Stent 3. One can see that at time $t = 7$ ms the reflected wave with the largest magnitude of displacement corresponds to the stiffest stent, namely Stent 3. At the same time the transmitted wave that travels through the stent, has the smallest

amplitude. The opposite is true for Stent 2: the largest amplitude of the transmitted wave traveling through the stent occurs for Stent 2. This is shown in red line in Figure 10 at $t = 7$ ms. The relatively large arterial wall displacement within the stent itself may cause larger strains within the arterial wall, which have been associated with potential for neointimal hyperplasia and in-stent restenosis. Further research needs to be performed to associate these finding with physiological implications.

We showed here the feasibility of our proposed methodology to capture the intricate properties of FSI between blood flow and arterial wall treated with a stent. The proposed methodology can then be used for more realistic scenarios in future research.

Numerical convergence. We conclude this section by showing the convergence rates in time for our extended Lie-splitting scheme. Figure 11 shows the log-log plot of the relative error in displacement (left panel) and velocity (right panel) versus time step. We compared the performance of the extended Lie splitting scheme (i.e., the β -scheme), described in Section 5.1, for $\beta = 0$ and $\beta = 1$. Solutions for different Δt were compared to the “reference solution”, which was obtained for $\Delta t = 5 \times 10^{-6}$. A plain straight artery without a stent was considered as a test case.

Figure 10 shows that the splitting scheme for $\beta = 0$ converges, and that the numerical accuracy of the scheme converges to 0.5, namely, that the relative error is of order $\mathcal{O}(\sqrt{\Delta t})$. For $\beta = 1$, however, we see that the splitting scheme converges, and that the scheme is first-order accurate in time, i.e., that the relative error is of order $\mathcal{O}(\Delta t)$. Details of the mathematical analysis related to the numerical accuracy of the β -scheme can be found in [15].

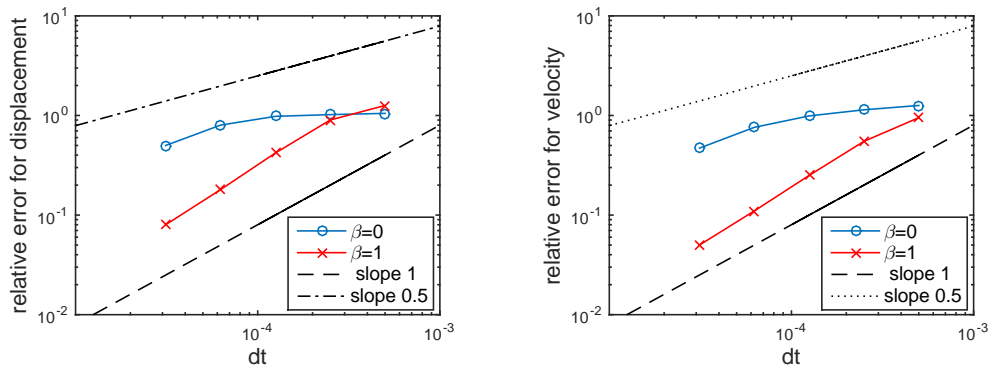


FIGURE 11. Convergence in time: comparison between $\beta = 0$ and $\beta = 1$. Left: displacement; Right: velocity. One can notice $\sqrt{\Delta t}$ -order convergence for $\beta = 0$, and Δt -order convergence for $\beta = 1$.

9. CONCLUSIONS

This work was motivated by FSI problems between blood flow and arterial walls treated with vascular prosthesis called stents. The Navier-Stokes equations for an incompressible viscous fluid were used to model the blood flow, and the cylindrical Kotier shell equations with discontinuous coefficients were used to model the elastic properties of arterial walls treated with stents. The FSI problem is set in 3D with no axial symmetry assumed in the model equations. The presence of a stent was modeled by the jump discontinuities in the structure coefficients.

We proved the existence of a weak solution to this nonlinear moving-boundary problem and designed a loosely-coupled partitioned numerical scheme for its solution. The main steps in the constructive existence proof were based on a time-discretization via operator splitting, which was then used in the design of the corresponding numerical scheme. Therefore, the existence proof effectively shows that the resulting numerical scheme converges to a weak solution to this nonlinear FSI problem.

The main novelties are in the design of an *extended Lie splitting* strategy which separates the fluid from structure sub-problems, and in the fact that we allow the coefficients of the structure to depend on the spatial variable and have jump discontinuity where the stent struts are located. The new operator

splitting strategy is based on distributing the entire normal fluid stress between the fluid and structure sub-problems in such a way that only one iteration between the fluid and structure sub-problems is necessary to achieve stability and convergence of the scheme, even when the fluid and structure densities are comparable. A parameter $\beta \in [0, 1]$ was introduced to distribute the normal fluid stress $\boldsymbol{\sigma}\mathbf{n}$: the portion $\beta\boldsymbol{\sigma}\mathbf{n}$ was used to load the structure, and the remaining portion $(1 - \beta)\boldsymbol{\sigma}\mathbf{n}$ was used in a Robin boundary condition for the fluid. It is the Robin boundary condition for the fluid sub-problem that makes the proposed splitting strategy stable. This is because the Robin condition involves the structure density, which makes it strongly coupled to the fluid density in the fluid sub-problem, thereby avoiding stability issues related to the added mass effect in classical loosely-coupled schemes [19]. The splitting of the normal stress only increases the accuracy of the scheme. We show numerically that for $\beta = 1$ the time-convergence of the scheme is of order 1, i.e., $\mathcal{O}(\Delta t)$, while for $\beta = 0$ the time-convergence is of order $\mathcal{O}(\sqrt{\Delta t})$. Our existence result shows that the numerical scheme converges to a weak solution for $\beta \in [0, 1)$. We mention that the compactness arguments that we constructed for $\beta \in [0, 1)$ could not be extended to the case $\beta = 1$. This is because our uniform “global” energy estimates depend on $(1 - \beta)$ and become useless when $\beta = 1$. The presented numerical simulations show, however, that our method converges even for $\beta = 1$. We believe that convergence for the case $\beta = 1$ can be proved by using a different mathematical approach, i.e., by considering a sequence of convergent solutions for different β and showing that as $\beta \rightarrow 1$ the sequence converges. Further research on this problem is under way.

We implemented the proposed numerical scheme and solved several numerical examples with different stent configurations. The results show that the presence of a stent introduces reflected waves in the arterial walls, and significant disturbances in the blood flow patterns. We considered three different stent configurations associated with three different overall stent stiffness properties, and showed that stiffer stents induce reflected waves with large amplitude and stronger disturbances in blood flow patterns. Further research is needed to correlate these findings with the well-known problems of in-stent restenosis associated with stiffer stent configurations.

We showed here a feasibility of our proposed methodology to capture the intricate properties of FSI between blood flow and arterial wall treated with a stent. The proposed methodology can then be used for more realistic scenarios in future research.

10. ACKNOWLEDGEMENTS

The authors would like to thank Frédéric Hecht and Olivier Pironneau for their help with FreeFem++. Special thanks are extended to the funding agencies: US National Science Foundation (grants DMS-1311709 (Canic and Bukac), DMS-1311709 (Canic and Muha), and DMS-1262385 (Canic)), the Croatian Science Foundation (Hrvatska Zaklada za Znanost; grant number 9477), and the UH Cullen Chair Funds (Canic).

REFERENCES

- [1] FreeFem++, Université Pierre et Marie Curie, Laboratoire Jacques-Louis Lions. <http://www.freefem.org/ff++/>.
- [2] A.R. Adams. *Sobolev spaces*. Academic Press [A subsidiary of Harcourt Brace Jovanovich, Publishers], New York-London, 1975. Pure and Applied Mathematics, Vol. 65.
- [3] M. Astorino, F. Chouly, and M.A. Fernández Varela. Robin based semi-implicit coupling in fluid-structure interaction: Stability analysis and numerics. *SIAM J. Sci. Comput.*, 31:4041–4065, 2009.
- [4] S. Badia, F. Nobile, and C. Vergara. Fluid-structure partitioned procedures based on Robin transmission conditions. *J. Comput. Phys.*, 227:7027–7051, 2008.
- [5] S. Badia, A. Quaini, and A. Quarteroni. Splitting methods based on algebraic factorization for fluid-structure interaction. *SIAM J. Sci. Comput.*, 30(4):1778–1805, 2008.
- [6] J. Banks, W. Henshaw, and D. Schwendeman. An analysis of a new stable partitioned algorithm for FSI problems. Part I: Incompressible flow and elastic solids. *Journal of Computational Physics*, 269:108–137, 2014.
- [7] J. Banks, W. Henshaw, and D. Schwendeman. An analysis of a new stable partitioned algorithm for FSI problems. Part II: Incompressible flow and structural shells. *Journal of Computational Physics*, 268:399–416, 2014.
- [8] V. Barbu, Z. Grujić, I. Lasiecka, and A. Tuffaha. Existence of the energy-level weak solutions for a nonlinear fluid-structure interaction model. In *Fluids and waves*, volume 440 of *Contemp. Math.*, pages 55–82. Amer. Math. Soc., Providence, RI, 2007.
- [9] V. Barbu, Z. Grujić, I. Lasiecka, and A. Tuffaha. Smoothness of weak solutions to a nonlinear fluid-structure interaction model. *Indiana Univ. Math. J.*, 57(3):1173–1207, 2008.

- [10] H. Beirão da Veiga. On the existence of strong solutions to a coupled fluid-structure evolution problem. *J. Math. Fluid Mech.*, 6(1):21–52, 2004.
- [11] L. Bociu, D. Toundykov, and J.-P. Zolésio. Well-posedness analysis for a linearization of a fluid-elasticity interaction. *SIAM Journal on Mathematical Analysis*, 47(3):1958–2000, 2015.
- [12] M. Bukac and S. Canic. Longitudinal displacement in viscoelastic arteries: a novel fluid-structure interaction computational model, and experimental validation. *Journal of Mathematical Biosciences and Engineering*. Accepted 2012.
- [13] M. Bukac, S. Canic, R. Glowinski, J. Tambaca, and A. Quaini. Fluid-structure interaction in blood flow capturing non-zero longitudinal structure displacement. *Journal of Computational Physics*, 235(0):515 – 541, 2013.
- [14] M. Bukac, S. Canic, and B. Muha. A partitioned scheme for fluid-composite structure interaction problems. *Journal of Computational Physics*, 281(0):493 – 517, 2015.
- [15] M. Bukac and B. Muha. Stability and convergence analysis of the kinematically coupled scheme and its extensions for the fluid-structure interaction. *Submitted*, 2015.
- [16] M. Bukac, I. Yotov, and P. Zunino. An operator splitting approach for the interaction between a fluid and a multi-layered poroelastic structure. *Numerical Methods for Partial Differential Equations*, 31(4):1054–1100, 2015.
- [17] S. Čanić, B. Muha, and M. Bukac. Fluid–structure interaction in hemodynamics: Modeling, analysis, and numerical simulation. In *Fluid-Structure Interaction and Biomedical Applications*, pages 79–195. Springer Basel, 2014.
- [18] S. Canic and J. Tambaca. Cardiovascular stents as PDE nets: 1D vs. 3D. *IMA J. Appl. Math.*, 77(6):748–770, 2012.
- [19] P. Causin, J. F. Gerbeau, and F. Nobile. Added-mass effect in the design of partitioned algorithms for fluid-structure problems. *Comput. Methods Appl. Mech. Engrg.*, 194(42-44):4506–4527, 2005.
- [20] T. Chacon-Rebollo, V. Girault, F. Murat, and O. Pironneau. Analysis of a simplified coupled fluid-structure model for computational hemodynamics. *to appear in SIAM journal on Numerical Analysis*.
- [21] A. Chambolle, B. Desjardins, M. J. Esteban, and C. Grandmont. Existence of weak solutions for the unsteady interaction of a viscous fluid with an elastic plate. *J. Math. Fluid Mech.*, 7(3):368–404, 2005.
- [22] C. H. A. Cheng, D. Coutand, and S. Shkoller. Navier-Stokes equations interacting with a nonlinear elastic biofluid shell. *SIAM J. Math. Anal.*, 39(3):742–800 (electronic), 2007.
- [23] C. H. A. Cheng and S. Shkoller. The interaction of the 3D Navier-Stokes equations with a moving nonlinear Koiter elastic shell. *SIAM J. Math. Anal.*, 42(3):1094–1155, 2010.
- [24] C.H. Ciarlet and D. Coutand. An existence theorem for nonlinearly elastic “flexural” shells. *J. Elasticity*, 50(3):261–277, 1998.
- [25] C.R. Ciarlet and A. Roquefort. Justification of a two-dimensional shell model of koiter type. *C.R. Acad. Sci. Paris, Ser I Math.* 331(5):411–416, 2000.
- [26] P. G. Ciarlet. A two-dimensional nonlinear shell model of koiter type. *C.R. Acad. Sci. Paris. Ser I Math.*, 331:405–410, 2000.
- [27] C. Conca, F. Murat, and O. Pironneau. The Stokes and Navier-Stokes equations with boundary conditions involving the pressure. *Japan. J. Math. (N.S.)*, 20(2):279–318, 1994.
- [28] D. Coutand and S. Shkoller. Motion of an elastic solid inside an incompressible viscous fluid. *Arch. Ration. Mech. Anal.*, 176(1):25–102, 2005.
- [29] D. Coutand and S. Shkoller. The interaction between quasilinear elastodynamics and the Navier-Stokes equations. *Arch. Ration. Mech. Anal.*, 179(3):303–352, 2006.
- [30] S. Deparis, M. Discacciati, G. Fourestey, and A. Quarteroni. Fluid-structure algorithms based on Steklov-Poincaré operators. *Comput. Methods Appl. Mech. Engrg.*, 195(41-43):5797–5812, 2006.
- [31] S. Deparis, M. Fernandez, and L. Formaggia. Acceleration of a fixed point algorithm for a fluid-structure interaction using transpiration condition. *Math. Model. Numer. Anal.*, 37(4):601–616, 2003.
- [32] J. Donea. Arbitrary lagrangian-eulerian finite element methods, in: *Computational methods for transient analysis. North-Holland, Amsterdam*, 1983.
- [33] Q. Du, M. D. Gunzburger, L. S. Hou, and J. Lee. Analysis of a linear fluid-structure interaction problem. *Discrete Contin. Dyn. Syst.*, 9(3):633–650, 2003.
- [34] C. Farhat, P. Geuzaine, and C. Grandmont. The discrete geometric conservation law and the nonlinear stability of ale schemes for the solution of flow problems on moving grids. *Journal of Computational Physics*, 174(2):669–694, 2001.
- [35] M. A. Fernández. Incremental displacement-correction schemes for incompressible fluid-structure interaction: stability and convergence analysis. *Numerische Mathematik*, 2012.
- [36] M.A. Fernández, J.F. Gerbeau, and C. Grandmont. A projection algorithm for fluid-structure interaction problems with strong added-mass effect. *C. R. Math.*, 342(4):279–284, 2006.
- [37] C. Figueroa, I. Vignon-Clementel, K. Jansen, T. Hughes, and C. Taylor. A coupled momentum method for modeling blood flow in three-dimensional deformable arteries. *Computer Methods in Applied Mechanics and Engineering*, 195(41-43):5685–5706, 2006.
- [38] L. Formaggia, J.F. Gerbeau, F. Nobile, and A. Quarteroni. On the coupling of 3d and 1d navier-stokes equations for flow problems in compliant vessels. *Comput. Methods Appl. Mech. Eng.*, 191(6-7):561–582, 2001.
- [39] R. Glowinski. *Finite element methods for incompressible viscous flow*, in: *P.G.Ciarlet, J.-L.Lions (Eds), Handbook of numerical analysis*, volume 9. North-Holland, Amsterdam, 2003.
- [40] C. Grandmont. Existence of weak solutions for the unsteady interaction of a viscous fluid with an elastic plate. *SIAM J. Math. Anal.*, 40(2):716–737, 2008.

- [41] C. Grandmont and M. Hillairet. Existence of global strong solutions to a beam-fluid interaction system. *arXiv preprint arXiv:1504.00830*, 2015.
- [42] G. Guidoboni, R. Glowinski, N. Cavallini, and S. Canic. Stable loosely-coupled-type algorithm for fluid-structure interaction in blood flow. *J. Comput. Phys.*, 228(18):6916–6937, 2009.
- [43] G. Guidoboni, M. Guidorzi, and M. Padula. Continuous dependence on initial data in fluid-structure motions. *J. Math. Fluid Mech.*, 14(1):1–32, 2012.
- [44] A. Hundertmark-Zaušková, M. Lukáčová-Medvidová, and G. Rusnáková. Fluid-structure interaction for shear-dependent non-Newtonian fluids. In *Topics in mathematical modeling and analysis*, volume 7 of *Jindřich Nečas Cent. Math. Model. Lect. Notes*, pages 109–158. Matfyzpress, Prague, 2012.
- [45] M. Ignatova, I. Kukavica, Irena L., and A. Tuffaha. On well-posedness for a free boundary fluid-structure model. *J. Math. Phys.*, 53(11):115624, 13, 2012.
- [46] M. Ignatova, I. Kukavica, I. Lasiecka, and A. Tuffaha. On well-posedness and small data global existence for an interface damped free boundary fluid–structure model. *Nonlinearity*, 27(3):467, 2014.
- [47] Igor K. and Amjad T. Solutions to a free boundary problem of fluid-structure interaction. *Indiana Univ. Math. J.*, 61:1817–1859, 2012.
- [48] W. T. Koiter. On the foundations of the linear theory of thin elastic shells. i, ii. *Nederl. Akad. Wetensch. Proc.*, Ser. B 73.
- [49] I. Kukavica and A. Tuffaha. Solutions to a fluid-structure interaction free boundary problem. *DCDS-A*, 32(4):1355–1389, 2012.
- [50] I. Kukavica and A. Tuffaha. Well-posedness for the compressible Navier-Stokes-Lamé system with a free interface. *Nonlinearity*, 25(11):3111–3137, 2012.
- [51] I. Kukavica, A. Tuffaha, and M. Ziane. Strong solutions for a fluid structure interaction system. *Adv. Differential Equations*, 15(3-4):231–254, 2010.
- [52] D. Lengeler. Global weak solutions for an incompressible, generalized newtonian fluid interacting with a linearly elastic koiter shell. arXiv:1212.3435, 2012.
- [53] D. Lengeler and M. Ružička. Global weak solutions for an incompressible newtonian fluid interacting with a linearly elastic koiter shell. arXiv:1207.3696v1, 2012.
- [54] J. Lequeurre. Existence of strong solutions to a fluid-structure system. *SIAM J. Math. Anal.*, 43(1):389–410, 2011.
- [55] J. Lequeurre. Existence of Strong Solutions for a System Coupling the Navier–Stokes Equations and a Damped Wave Equation. *J. Math. Fluid Mech.*, 15(2):249–271, 2013.
- [56] A. Hundertmark-Zaušková M. Lukáčová-Medvid'ová, G. Rusnáková. Kinematic splitting algorithm for fluidstructure interaction in hemodynamics. *Computer Methods in Appl. Mech. Engi.*, To appear., 2013.
- [57] B. Muha. A note on the trace theorem for domains which are locally subgraph of a Hölder continuous function. *Netw. Heterog. Media*, 9(1):191–196, 2014.
- [58] B. Muha and S. Čanić. A nonlinear, 3d fluid-structure interaction problem driven by the time-dependent dynamic pressure data: a constructive existence proof. *Communications in Information and Systems*, 13(3):357–397, 2013.
- [59] B. Muha and S. Čanić. Existence of a solution to a fluid–multi-layered-structure interaction problem. *J. Differential Equations*, 256(2):658–706, 2014.
- [60] B. Muha and S. Canic. Existence of a weak solution to a fluid-elastic structure interaction problem with the navier slip boundary condition. *arXiv preprint arXiv:1505.04462*, 2015.
- [61] B. Muha and S. Čanić. Fluid-structure interaction between an incompressible, viscous 3d fluid and an elastic shell with nonlinear koiter membrane energy. *Interfaces and free boundaries*, 2015.
- [62] B. Muha and S. Čanić. Existence of a Weak Solution to a Nonlinear Fluid–Structure Interaction Problem Modeling the Flow of an Incompressible, Viscous Fluid in a Cylinder with Deformable Walls. *Arch. Ration. Mech. Anal.*, 207(3):919–968, 2013.
- [63] C.M. Murea and S. Sy. A fast method for solving fluid-structure interaction problems numerically. *Int. J. Numer. Meth. Fl.*, 60(10):1149–1172, 2009.
- [64] F. Nobile and C. Vergara. An effective fluid-structure interaction formulation for vascular dynamics by generalized Robin conditions. *SIAM J. Sci. Comput.*, 30:731–763, 2008.
- [65] A. Quarteroni, M. Tuveri, and A. Veneziani. Computational vascular fluid dynamics: problems, models and methods. survey article. *Comput. Visual. Sci.*, 2:163–197, 2000.
- [66] J.-P. Raymond and M. Vanninathan. A fluid–structure model coupling the navier–stokes equations and the lamé system. *Journal de Mathématiques Pures et Appliquées*, 102(3):546–596, 2014.
- [67] J. Simon. Compact sets in the space $L^p(0, T; B)$. *Ann. Mat. Pura Appl. (4)*, 146:65–96, 1987.
- [68] J. Tambača, M. Kosor, S. Čanić, and D. Paniagua. Mathematical modeling of vascular stents. *SIAM J. Appl. Math.*, 70(6):1922–1952, 2010.
- [69] R. Temam. Sur la résolution exacte et approchée d'un problème hyperbolique non linéaire de T. Carleman. *Arch. Rational Mech. Anal.*, 35:351–362, 1969.
- [70] S. Čanić, B. Muha, and M. Bukač. Stability of the kinematically coupled β -scheme for fluid-structure interaction problems in hemodynamics. *Int J Numer Anal Model*, 12(1):54–80, 2015.

UNIVERSITY OF NOTRE DAME
E-mail address: `mbukac@nd.edu`

UNIVERSITY OF HOUSTON
E-mail address: `canic@math.uh.edu`

UNIVERSITY OF ZAGREB
E-mail address: `boris@math.hr`